Metal artifact reduction strategies for improved attenuation correction in hybrid PET/CT imaging

Mehrsima Abdoli and Rudi A. J. O. Dierckx
Department of Nuclear Medicine and Molecular Imaging, University of Groningen, University Medical Center Groningen, 9700 RB Groningen, The Netherlands

Habib Zaidi[a)]
Division of Nuclear Medicine and Molecular Imaging, Geneva University Hospital, CH-1211 Geneva, Switzerland; Geneva Neuroscience Center, Geneva University, CH-1205 Geneva, Switzerland; and Department of Nuclear Medicine and Molecular Imaging, University of Groningen, University Medical Center Groningen, 9700 RB Groningen, The Netherlands

(Received 23 October 2011; revised 31 March 2012; accepted for publication 10 April 2012; published 24 May 2012)

Metallic implants are known to generate bright and dark streaking artifacts in x-ray computed tomography (CT) images, which in turn propagate to corresponding functional positron emission tomography (PET) images during the CT-based attenuation correction procedure commonly used on hybrid clinical PET/CT scanners. Therefore, visual artifacts and overestimation and/or underestimation of the tracer uptake in regions adjacent to metallic implants are likely to occur and as such, inaccurate quantification of the tracer uptake and potential erroneous clinical interpretation of PET images is expected. Accurate quantification of PET data requires metal artifact reduction (MAR) of the CT images prior to the application of the CT-based attenuation correction procedure. In this review, the origins of metallic artifacts and their impact on clinical PET/CT imaging are discussed. Moreover, a brief overview of proposed MAR methods and their advantages and drawbacks is presented. Although most of the presented MAR methods are mainly developed for diagnostic CT imaging, their potential application in PET/CT imaging is highlighted. The challenges associated with comparative evaluation of these methods in a clinical environment in the absence of a gold standard are also discussed. © *2012 American Association of Physicists in Medicine*. [http://dx.doi.org/10.1118/1.4709599]

Key words: x-ray CT, PET/CT, attenuation correction, metal artifacts, metal artifact reduction

I. INTRODUCTION

X-ray computed tomography (CT) has been widely used for decades as a high-throughput, high-resolution, and low-noise imaging modality which provides reliable anatomical information.[1] However, the application of CT in oncology suffers from the lack of functional information which makes the differentiation between malignant and nonmalignant tissue challenging.[2] Moreover, after radiotherapy or surgical tumor removal, evaluation of the treatment using standalone CT has been problematic owing to tissue deformation.[3,4]

On the other hand, positron emission tomography (PET) has been considered as a powerful molecular imaging modality which has gained wide clinical acceptance during the last two decades.[5] PET is capable of identifying functional changes at the cellular level in an early stage well before the appearance of anatomical changes. However, these functional changes can hardly be localized using standalone PET scanners. Hence, the combination of these two imaging modalities was considered to compensate for the shortcomings of each modality.[6,7]

Today, PET/CT is widely used in oncology staging and follow-up of various cancers such as lung and head-and-neck,[8] lymphoma, melanoma, and gastrointestinal malignancies,[9] and abdominal and pelvic cancers.[10] PET/CT provides accurate localization of the metabolic abnormalities and has improved cancer staging and patient management.[2,11] Patient management can be optimized by tailoring the treatment for each individual patient.[12] PET/CT might also improve quantification of PET data, thus allowing more accurate assessment of tissue metabolism, radiation dosimetry calculations, and myocardial perfusion measurements.[13] Another advantage of dual-modality imaging is lower acquisition time, which leads to higher patient throughput.[14] It has also been reported that compared to CT-alone and PET-alone, PET/CT improves the accuracy, sensitivity, and specificity of malignant tissue detection.[2,11] In addition to the above-mentioned advantages of combined PET/CT imaging, CT images can also be utilized as a low-noise attenuation map for attenuation correction of PET data.[15]

It is well established that attenuation correction of PET data plays a pivotal role to prevent false decrease of tracer uptake particularly in deep regions within the body.[16] Traditional transmission scans provide noisy attenuation maps which add noise to attenuation corrected PET images.[17] Long scanning times also cause patient inconvenience and increase patient motion probability.[18] However, CT images provide attenuation coefficients of biological tissues for photons at the corresponding effective energy of the x-ray spectrum of the CT scanner.[19] These attenuation coefficients are

usually converted to the 511 keV for PET to generate an attenuation map for CT-based attenuation correction (CTAC).[18,20]

In spite of the considerable advantages of CTAC, the technique suffers from the propagation of possible pitfalls and artifacts of CT images to the corresponding PET images.[18,21–23] Moreover, cardiac and respiratory motion results in mismatch in the position of organs in the chest area between the CT and the corresponding PET images.[24–26] Typical artifacts associated with CT images that are likely to propagate to the corresponding attenuation corrected PET images include artifacts caused by intravenous or oral contrast media, truncation artifacts, and metal-induced artifacts.[27–32]

Metallic artifacts are quite common in CT images of patients who have permanent metallic implants such as dental fillings, hip or knee prostheses, cardiac pacemakers.[27] About 10% of CT images involve extracranial metal artifacts.[33] Due to the high atomic number of metallic objects, x-ray photons passing through these objects are highly attenuated and result in gaps in the projection data. Reconstruction of these incomplete projection data generates bright and dark streaking artifacts in the reconstructed CT image.[34,35] The presence of these streaks not only deteriorates the quality of the CT image but also results in erroneous CTAC of corresponding PET images. The latter causes inaccurate quantification of tracer uptake, which might appear in the form of either overestimation or underestimation of the actual activity concentration.[36–38] Therefore, metal artifact reduction of CT images prior to application of the CTAC procedure is recommended in most of the cases.[39] In this paper, metal artifact reduction techniques proposed for application on either standalone CT or combined PET/CT scanners are described. Since the majority of the proposed methods are specifically designed for CT imaging, their performance in the context of CTAC of PET data is discussed and documented through experience gathered from techniques assessed for this particular application. The functionality of these algorithms is assessed based on accuracy, ease of use, and the potential application for CTAC of PET images.

II. METAL ARTIFACTS IN X-RAY CT AND PET/CT

Several causes have been reported as potential origins of streak artifacts. Beam hardening effect,[40] Compton scattering,[41] noise,[42] axial partial volume effect,[43] and object motion[44] have been reported in the literature as some of the possible causes of streak artifacts. De Man *et al*. performed simulation studies to assess the influence of all these factors on the generation of streak artifacts in the presence of metallic objects.[45] They developed a realistic CT simulator incorporating all the geometrical parameters and physical properties of a clinical commercial CT scanner based on 2D fan-beam geometry. In particular, the possibility of switching on and off artifact generating factors such as beam hardening, scatter, and noise enables to understand the main cause of metal-related streaking artifacts. They also simulated different phantoms containing metallic inserts of different size. It has been shown that metal streaking artifacts can be most prominently attributed to a combination of the phenomena of noise, beam hardening, axial partial volume effect, and scatter.[27]

Noise can be defined as statistical fluctuations on the measurements which cause bright and dark streaks after reconstruction using conventional filtered backprojection. The severity of these streaks is more pronounced in the directions where the projection is more attenuated. This is due to the fact that the signal-to-noise ratio (SNR) of the projection data is relatively lower in those directions.

Beam hardening is the absorption of low-energy photons in a polychromatic x-ray beam while it passes through matter owing to the higher linear attenuation coefficient for low photon energies in the x-ray spectrum. Therefore, hard beams are less attenuated, and as such, the total attenuation of a polychromatic beam, which passes through a given material, is not strictly proportional to its thickness.[46] When this effect is neglected, beam hardening artifacts, in the form of bright and dark streaks, will be generated. This artifact is more visible along the projections which pass through densely attenuating materials.

The partial volume effect is present when a voxel of an image is partially filled with a certain material. The reconstructed voxel will then represent the weighted average of the attenuation of all materials present in that voxel. Since the axial spatial resolution is normally lower than the in-plane resolution, this effect is more severe in the axial direction. The consequence of this effect is that, first, the reconstructed attenuation of a partial volume element underestimates the average of attenuation of the materials included in the element, and second, in the presence of two or more partial volume elements, angle-dependent errors occur which are more pronounced along the lines which connect those elements. Such inconsistency results in streaking artifacts along the lines which connect the partial volume elements.[43,47] Compton scattering of photons has a similar behavior to beam hardening effect in the sense that the above-mentioned quantity is not a function of the path length in the presence of scatter. The resulting streaking artifacts in the direction of highest attenuation are also similar to the beam hardening artifacts.[48]

Some or all of the above-mentioned effects are usually present during clinical CT scanning, and as such, streaking artifacts are almost always produced in the presence of high attenuating materials. Metallic objects further amplify these artifacts. These streaks degrade the quality of CT images and deteriorate tissue attenuation properties in the attenuation map. Application of such corrupted attenuation map during CTAC results in over- and/or underestimation of tracer uptake in regions corresponding to streaking artifacts [36,49–51] (Fig. 1). Figure 2 illustrates how metal artifact reduction of CT images prior to CTAC affects the visual quality of attenuation corrected PET images.[52]

Although moderate streak artifacts produced by small metallic objects, such as fine dental fillings and EEG electrodes, might not influence the visual quality of the attenuation corrected PET images,[38,53] the produced artifacts are usually

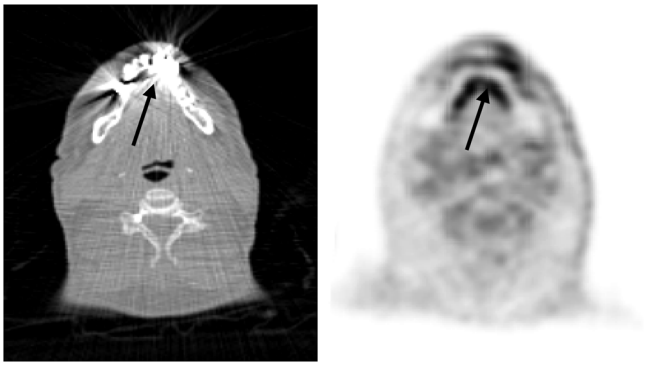

(a) (b)

FIG. 1. The influence of metal streaking artifacts on CT-based attenuation corrected PET image. (a) CT image with metal artifacts caused by dental fillings and (b) the corresponding attenuation corrected PET image. The arrows show the location of artifacts which have caused high activity uptake in the PET data.

strong enough to bias quantification of PET data in regions corresponding to the streaking artifacts.[38] Dental metallic implants have been reported as a common source of streaking artifacts in CT images, which may cause false-positive and/or false-negative findings in the attenuation corrected PET images.[54–56] The larger metallic implants such as hip and knee implants are more prone to generate strong artifacts and obscure the diagnostic information in CT images.[57–59] Total hip or knee replacements are likely to cause local complications whose diagnosis might be influenced by the strong streaking artifacts in the attenuation corrected PET data.[60,61] Cardiac pacemakers and implantable cardioverter defibrillators (ICDs) have also proven to be a source of streaking artifacts in CT images. However, only ICDs have been shown to cause significant bias in tracer uptake after CTAC.[62,63]

Artifacts generated from metallic implants can be troublesome for treatment planning in radiation therapy since it may impact dose distribution calculations[64] and divert tumor control probability and normal tissue complication probability.[65] To prevent the severe outcomes of metallic artifacts in the clinical practice, removable metallic objects are usually taken off. However, the major artifacts are produced by irremovable objects.[66] Therefore, extra effort is required to resolve this deficiency. In Sec. III, techniques proposed to deal with metallic artifacts are reviewed.

III. METAL ARTIFACT REDUCTION

During the past three decades, various approaches have been proposed for elimination or at least reduction of the undesirable effects caused by metallic implants on both CT and PET/CT images. These approaches are generally referred to as metal artifact reduction (MAR) techniques. There have been a few attempts to suppress these artifacts without the use of algorithmic mathematical MAR approaches. These approaches are referred to as implicit methods. The majority of the proposed approaches, however, are based on various mathematical algorithms. They are referred to in this paper as explicit MAR methods. The main characteristics and limitations of different MAR methods, belonging to these categories and associated subcategories, are summarized in Table I.

III.A. Implicit MAR methods

Coolens and Childs investigated the influence of using an extended CT scale on radiotherapy treatment planning of patients with metallic hip implants.[67] Scaling down the CT numbers, which expands the CT scale, enables the user to distinguish between the metallic object and surrounding tissues and also between high-density and low-density

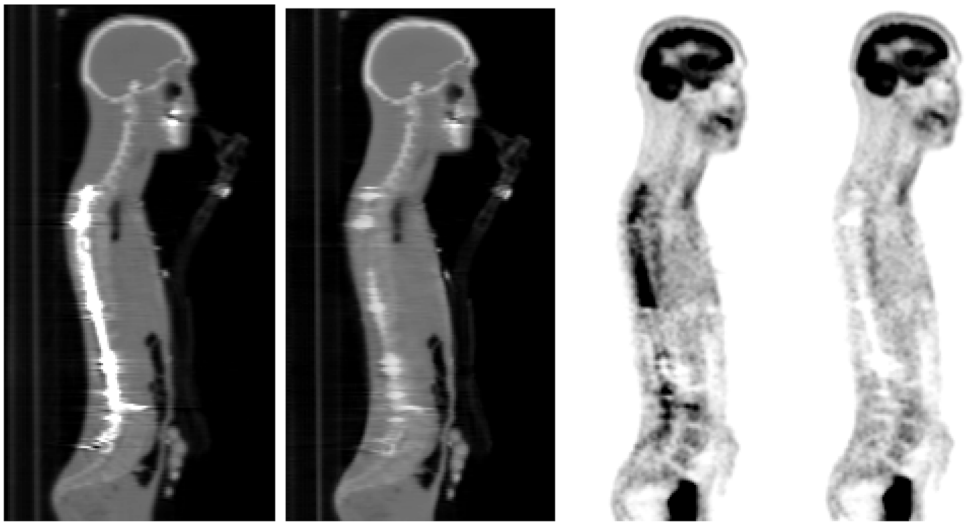

(a) (b) (c) (d)

FIG. 2. The influence of metal streaking artifacts and its correction on CT-based attenuation corrected PET image. (a) Original CT image, (b) corrected CT image, (c) PET image attenuation corrected by (a), and (d) PET image attenuation corrected by (c). Reprinted with permission from J. Nuyts and S. Stroobants, "Reduction of attenuation correction artifacts in PET-CT," in IEEE Nuclear Science Symposium Conference Record (Puerto Rico, 2005), Vol. 4, pp. 1895–1899. © 2005 IEEE.

TABLE I. Summary of main characteristics and limitations of different categories and subcategories of MAR methods.

Category	Characteristics	Limitations
Implicit methods	Manipulation of the parameters prior to the scanning procedure	Limited applicability
Explicit methods		
Interpolation-based sinogram correction	Fast and straightforward	Might cause extra artifacts
Noninterpolation-based sinogram correction	Various approaches to replace the affected projection bins	The influence on the attenuation corrected PET data has not been investigated
Iterative image reconstruction	The raw data are not manipulated No extra artifact is introduced	High computational time and the subsequent high costs
Hybrid sinogram correction		
Combination of interpolation- and noninterpolation-based sinogram correction	Compensate for one single method's shortcomings	The limitations are case dependant
Combination of interpolation-based sinogram correction and iterative reconstruction	Improve the quality of the corrected CT image compared to the methods which use FBP reconstruction	The inherent limitations of iterative approaches are still present; the quantitative impact has not been assessed
Combination of noninterpolation-based sinogram correction and iterative reconstruction	Improve the quality of the corrected CT image compared to the methods which use FBP reconstruction	The inherent limitations of iterative approaches are still present; the quantitative impact has not been assessed
Image-based approaches	The raw data are not manipulated. The affected pixels are replaced, usually by a constant value	Challenging task of differentiation between the metallic objects, artifactual regions and the surrounding tissues; do not account for underestimations

prostheses, thus allowing the accurate derivation of metallic object's electron density. However, this method does not deal with streaking artifacts caused by the implants owing to the simplicity of the approach which assumes that the implants are surrounded by soft tissues whose effective atomic numbers are close to water. Therefore, this method can only be utilized in the context of this specific application and cannot be considered as a general MAR technique.

The influence of technical scanning parameters on the produced metal artifacts has also been assessed.[68,69] Theoretically, improving the x-ray beam penetration by increasing tube voltage and current would reduce beam attenuation, thus suppressing metallic artifacts. It was reported that applying a higher tube voltage (100–120 kVp) is more effective for reducing the streak artifacts in the reconstructed CT images than increasing the tube current defined in terms of effective mAs.[69] However, a standard tube voltage of 120 kVp can still cause strong streaking artifacts in CT images.[56,59,62]

The use of dual-energy CT for MAR has also been considered.[70] This approach allows the extrapolation of beam hardening to obtain an image similar to the assumed image which would be acquired by a monoenergetic beam with high energy quanta. The results seem to suggest that when application of dual-energy CT is possible without substantially increasing patient dose, metallic artifacts can be significantly reduced. Another study aiming to reduce metallic artifacts caused by dental impression materials reported on the use of additional silicone material as a tooth shield.[71] This shielding is meant to decrease the abrupt change between the metal components and the surrounding structures. The results showed that the silicon shielding can effectively reduce dental metallic artifacts. Nevertheless, the physical explanation of this phenomenon is not clear yet and requires further investigation. Moreover, application of such shielding for other metallic implants used in different regions of the body might not always be feasible. Therefore, this method cannot be considered as a viable MAR technique.

Although implicit methods might have added value in some specific cases, they cannot be considered as ultimate MAR techniques. More general approaches are needed to accurately deal with different types of metal artifacts commonly produced by standard protocols used on clinical CT and PET/CT scanners.

III.B. Explicit MAR methods

Explicit MAR methods are at the forefront and have been the main focus of research groups during the past three decades. Various approaches have been proposed which can be classified in different ways. The majority of techniques operate on the raw CT projection data or in the sinogram domain. Other techniques incorporated the correction within an iterative reconstruction algorithm. A small proportion of the methods, though, prefer to handle the artifacts in the image domain. For better understanding of the working principles of these methods, we classified them into five main categories: interpolation-based sinogram correction, noninterpolation-based sinogram correction, hybrid sinogram correction, iterative image reconstruction, and image-based approaches. The principles of these methods are explained in Secs. III.B.1 to III.B.5.

III.B.1. Interpolation-based sinogram correction

A large proportion of proposed methods belong to this category. Lewitt and Bates developed the first interpolation-based sinogram correction MAR technique.[72] Several

groups followed almost the same procedure and implemented various interpolation techniques to improve the algorithm.[44,73–88] The main idea is to find projection bins affected by the metallic objects in the raw projection data and to replace the corrupted values by appropriate estimates. Figure 3 illustrates the general flowchart of these MAR approaches. Two approaches have been utilized for the detection of affected bins. The first approach localizes the affected bins directly in the sinogram domain. In this approach, the affected bins are distinguished because their intensities are higher than the other bins owing to the higher attenuation of metallic objects. The second approach segments the metallic objects from the image and forward project the binary image to obtain the position of the affected projection bins.

Some groups adopted the first detection approach in their MAR method, referred to as projection completion.[44,89] The values of the detected projection bins are substituted by fitting a polynomial function to at least one unaffected sample adjacent to the edges of the affected bins. The corrected image is obtained by filtered backprojection of the interpolated sinogram. In an attempt to improve the method of Lewitt and Glover, Hinderling *et al.* used the same detection approach and applied the linearly interpolated projections as a first approximation to correct the measured projection data.

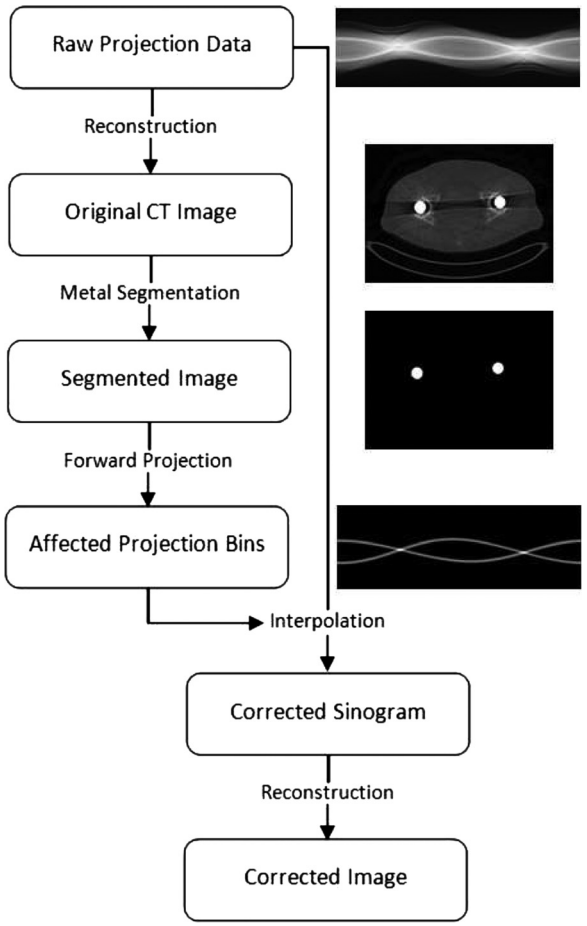

FIG. 3. General flowchart of interpolation-based sinogram correction MAR methods.

To improve the results obtained by linear interpolation, which causes a slight distortion in the reconstructed CT images owing to inconsistency in the affected projections, the following steps are employed: the cross sections of metallic objects are obtained by simple backprojection of the detected projection bins.[73] Thereafter, a uniform intensity (slightly higher than soft tissue) is assigned to the cross sections and the corresponding projections are calculated. The obtained values are added to the values calculated by linear interpolation of the unaffected projection bins and the corrected image is reconstructed. More recently, Veldkamp *et al.* again applied the first detection method and identified the affected bins in the sinogram space using a Markov random field-based segmentation.[87] Three different interpolation schemes have been used in their approach, including linear interpolation in each column of the sinogram matrix, a smooth interpolation using Laplace equation, and linear interpolation between the two corresponding projected edges belonging to the same object.

Kalender *et al.*, however, made use of the second detection approach, in which the objects are manually identified in the reconstructed CT image and the corresponding affected projection bins generated by forward projection of the segmented image using the CT scanner's geometry. The new values of the detected projections are calculated using a linear interpolation technique. As pointed out by the authors, this approach has a lower computational demand compared to previous interpolation-based approaches. Similar approaches using either manual or automatic thresholding-based segmentation of the metallic objects have been proposed. The only difference between these methods is the interpolation scheme used for replacing the values of the corrupted projection bins. These included cubic interpolation,[76,80] inpainting based on Euler's elastica and curvature,[79] total variation inpainting,[83] spline interpolation,[85] and two-dimensional Clough-Tocher cubic interpolation.[90] The latter introduced the concept of virtual sinogram to overcome the challenges pertaining to manipulation of raw CT data, such as large data size, and manufacturer-specific and encrypted proprietary format. In this approach, a virtual sinogram is obtained by forward projection of the reconstructed image according to the actual CT scanner geometry.

In addition, many worthwhile efforts focused on the improvement of the performance of the above-mentioned methods through the use of more sophisticated procedures. Zhao *et al.* proposed to incorporate extra information, obtained from the wavelet transform of the sinograms, to the interpolation procedure.[74] The MAR procedure starts with thresholding to extract metallic objects and setting other regions to zero and reprojection of the metal-only image (g_β^M) followed by linear interpolation of the affected projection bins (g_β^L). Thereafter, the wavelet transform of the original sinogram (g_β) and the summed sinogram $g_\beta^M + g_\beta^L$ is calculated and new wavelet coefficients are obtained by interpolation between the two wavelet transforms. The resulting coefficients are then reconstructed to generate the corrected image.

A two-dimensional interpolation scheme was proposed by Mahnken *et al*.[75] The authors used 16 reliable data points around each affected projection bin with a distance of less than a given value. Wei *et al*. investigated the influence of isolating bone structures using thresholding on the reduction of extra bone artifacts during the MAR procedure.[77] They applied polynomial interpolation to the bone-isolated sinogram, and after reconstruction of the corrected sinogram, they replaced the pixel values of bone structures and metallic objects. To determine the edges of the affected projection bins more precisely, Yazdi *et al*. used the gradient of the projections.[78] Thereafter, a linear interpolation is applied between the two edges belonging to the same object. The same group developed a nearest-neighbor interpolation technique for replacement of affected projection bins.[91] In this approach, each affected projection bin detected by thresholding and forward projection of the metallic object is replaced by its corresponding unaffected bin in a nearest slice. A good approximation for this correspondence is the projection on the opposite side ($\sim$180° apart).

Another new approach was proposed by Yu *et al*. in which metallic objects are segmented using the mean shift technique, which is a popular technique in the field of computer vision.[81] After reprojection of the segmented image, a feedback-based strategy is applied to adjust the interpolated value based on the prior knowledge that the interpolated values should not be larger than the original ones.

Manipulating the reformatted projections formed by combining the projection data at the same view angle over the full longitudinal scan range was suggested by Yu *et al*.[84] This reformatting provides coronal view of images at each slice. Therefore, in the case of hip implants, the whole metallic implant is visible on each slice. A Sobel edge detector was applied to delineate the borders of the metallic object, and a two-dimensional interpolation-based on Delaunay triangulation was used to replace the values of the affected projection bins. This approach was improved later using a dual-front active contour model to detect the boundaries of the metallic objects in the reformatted images.[92] Kim *et al*. identified the neighboring projection bins which are relevant to the target bin in a parallel beam projection setting.[86] Based on the distance between the target pixel and the neighboring relevant pixel, a Gaussian weight is assigned to the neighboring pixels to reduce interpolation errors. A linear interpolation performed on a normalized sinogram using forward projection of a prior image has been introduced by Meyer *et al*.[93] The prior image is obtained by a multithreshold segmentation of the original image. After applying the interpolation, the sinogram is denormalized and the corrected image is reconstructed.

Xu *et al*. proposed an algorithm for reduction of artifacts caused by permanent seed implants used in brachytherapy in order to enhance the accuracy of dose calculation.[88] Since small seeds can be implanted quite close together, using a fixed threshold for segmentation of metallic objects might result in merged objects. Therefore, a multithresholding process is used to decompose the merged objects into individual objects. Thereafter, Steger's method, which makes use of curvilinear property of the traces with subpixel accuracy,[94] is used to determine the position of the seed traces precisely in the sinogram domain. Finally, a linear interpolation is applied to the detected bins and the corrected image is reconstructed.

Most recently, Mehranian *et al*. presented a projection completion approach in which the interpolation of the affected projection bins is formulated as a constrained optimization in a Bayesian framework.[95] The authors used a wavelet-based prior to optimize the two-dimensional interpolation problem. This method employs sparsity constraints in contrast to the wavelet-based approach proposed by Zhao *et al*. which interpolates the wavelet coefficients.[74] Figure 4 illustrates a sample result of this category of MAR methods.[85] As can be seen, the interpolation technique has reduced the streaking artifacts in the corrected CT image

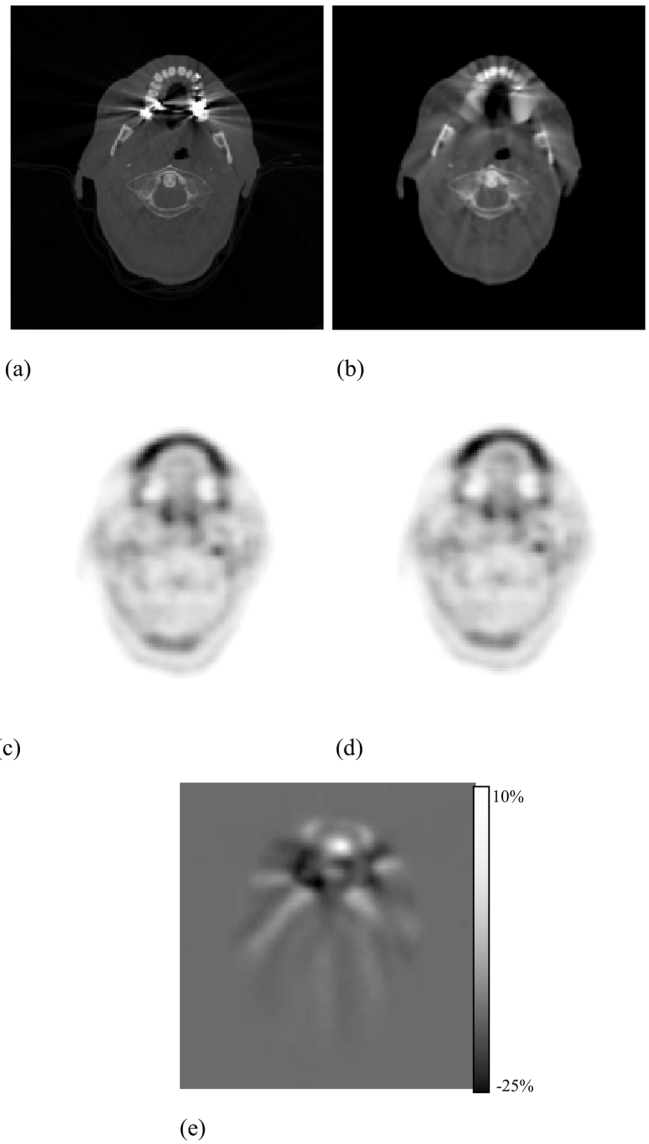

FIG. 4. A sample result of interpolation-based sinogram correction MAR methods (Ref. 125). (a) Original CT image including dental metallic artifact, (b) corrected CT image, (c) attenuation corrected PET data using image (a), (d) attenuation corrected PET data using image (b), and (e) subtraction of images (c) and (d).

[Fig. 4(b)]. However, the anatomical structures surrounding the dental fillings are oversmoothed and extra artifacts are introduced to the unaffected regions of the image. Nevertheless, using the corrected CT image for CTAC of PET data is effective for reducing overestimation and underestimation caused by bright and dark streaking artifacts to some extent [Fig. 4(e)].

III.B.2. Noninterpolation-based sinogram correction

Beside MAR techniques which exclusively correct the affected projection bins in the sinogram domain using an interpolation method, other approaches make use of other correction strategies in the sinogram domain. Morin and Raeside developed a MAR technique whose performance was assessed using Monte Carlo simulation studies.[96] In this approach, the projection bins intersecting the metallic objects are determined on the simulated raw data and a nearest-neighbor pattern recognition approach[97] is utilized to modify the values of the affected projections. Liu *et al.* detected the affected projections in the sinogram space in two steps:[98] First, since the affected projections are expected to have higher intensities than the surrounding projections, the highly probable affected projections are determined using thresholding. Thereafter, a set of sinusoidal curves are fitted to the identified projections to determine the complete set of affected projection bins. In this way the detected projections which do not belong to the sinusoidal curve, and thus do not fit in the affected projections, are eliminated. The sinogram is then amended in the identified region by subtracting a value which depends on the attenuation coefficient of the metallic object and the maximum intensity in each projection angle. This procedure results in a lower intensity of the affected projection bins, and as such streaking artifacts are reduced in the reconstructed image.

A projection replacement approach was proposed by Bal and Spies who used a tissue-class modeling of the distorted image.[99] Using a k-means clustering technique, the adaptively filtered image is segmented into different classes including air, soft tissue, normal tissue, bone and metal. The CT number of metallic regions is then converted to that of the surrounding material and the resulting model forward projected to obtain a model sinogram. The metal class is also separately forward projected to determine the affected projections, which are then replaced by the corresponding projections in the model sinogram. A similar approach has been applied by Wu *et al.* in which they assigned a weighting coefficient to the model sinogram, and the complementary weighting coefficient was assigned to the original sinogram.[100]

In another approach, Cheng and Liu applied a bilateral filter to the reconstructed image, in which the segmented metallic objects had been temporarily replaced by pixel values of the neighboring soft tissues.[101] Forward projection of the filtered image results in new values for the projection bins affected by metallic objects. In the end, the segmented metallic objects are superimposed on the reconstructed image.

More recently, Mehranian *et al.* developed a MAR approach based on Bayesian iterative image restoration in the sinogram domain.[102] The authors use a Sobolev prior in the maximum *a posteriori* estimation of the affected projection bins. Figure 5 illustrates how this approach corrects for metallic artifacts present in CT images. It can be clearly seen that the anatomical structures around metallic objects are satisfactorily preserved.[102]

III.B.3. Iterative image reconstruction

Until recently, virtually all scanner manufacturers used filtered backprojection (FBP) algorithms for CT image reconstruction.[103] The FBP method assumes that the projection data are consistent and complete. However, this is not the case when a high-density object is present. Therefore, there have been several attempts to alleviate the reconstruction deficiency using either the exterior Radon transform[104] or iterative reconstruction approaches. Since photon starvation is not the only origin of metal streaking artifacts (as discussed in Sec. II), an improved reconstruction technique will not necessarily remove visible artifacts. Otherwise, one would expect to obtain an artifact-free image using iterative reconstruction, which is not the case as will be discussed in details in Sec. III.B.4.c.

Iterative techniques are common in problems that involve optimization. The reconstruction problem can be considered a particular case where the aim is to determine the "best" estimate of the object based on the measured projections. Iterative reconstruction techniques include two main groups: algebraic and statistical techniques.[105] Examples of the first group are the algebraic reconstruction technique (ART) and the simultaneous iterative reconstruction technique (SIRT).[106] The best known example of the second group is the maximum likelihood-expectation maximization (ML-EM) algorithm.[107,108]

Iterative deblurring using the ML-EM formulation and the SIRT technique has been applied to suppress metallic artifacts.[34,109–111] The ML-EM method consists of the following steps: first, an initial guess image is assumed and then reprojected to obtain the estimated projections. Thereafter, the measured projection data are divided by the

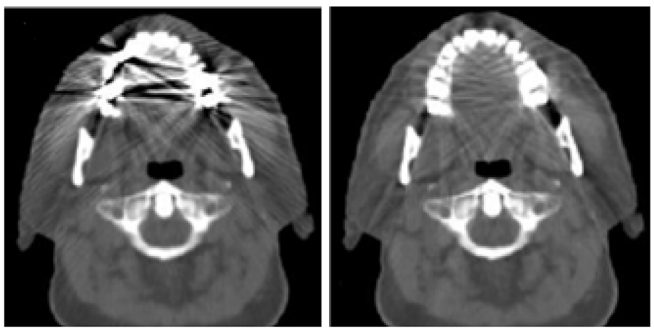

FIG. 5. A sample result of noninterpolation-based sinogram correction MAR methods. (a) Original CT image including dental metallic artifact, (b) corrected CT image. Reprinted with permission from A. Mehranian, M. R. Ay, A. Rahmim and H. Zaidi, "Metal artifact reduction in CT-based attenuation correction of PET using Sobolev sinogram restoration," in IEEE Nuclear Science Symposium and Medical Imaging Conference (Valencia, Spain, 2011), pp. 2936–2942. © 2005 IEEE.

corresponding estimated data and the obtained ratio is backprojected to form a multiplicative correction image. The resulting image is then multiplied by the current estimate to obtain the new estimate. It is also necessary to normalize for the number of contributions to the correction image, hence the division by a factor representing the backprojection of every possible line of response. These steps are repeated until the iteration converges to an acceptable range of error.[112] In the SIRT method, the same procedure is followed, except that the discrepancy between the measured and estimated projection data is calculated by subtraction instead of division.[106]

De Man *et al*. applied a statistical iterative reconstruction algorithm, referred to as the transmission maximum likelihood (ML-TR) technique.[113] The algorithm uses the Markov random field smoothness prior[114] and reconstructs the images at double resolution to provide sharp edges and better handling of other sources of errors, such as beam hardening and partial volume effect. After the last iteration the image is down-sampled to its normal resolution. The ML-TR algorithm optimizes the likelihood under the assumption that the detector readouts have a Poisson distribution. Therefore, less weight is assigned to low-count readouts.[115] An iterative MAR approach was proposed by Hsieh *et al*.[116] for cone beam CT that uses tilted parallel beam geometry as an estimation of the cone beam geometry. Using a sequence of mathematical formulations, it has been shown that the error introduced to the projections is approximately proportional to the line integral of the high-density materials along the projection path. The error is estimated by forward projection of the segmented high-density materials. Thereafter, the error is subtracted from the original measured projection data and the resulting projections are reconstructed. This procedure can be performed iteratively to obtain lower projection errors. Williamson *et al*. presented another statistical iterative reconstruction technique, called alternating minimization (AM), in which the prior information concerning the geometry of metallic objects and the statistical model of detector response are used.[117] The algorithm also accounts for the beam hardening and scattering effect.[118]

Boas and Fleischmann[119] proposed a selective algebraic reconstruction technique (SART). This is an iterative reconstruction algorithm in which all the projection data are used to reconstruct the metal regions, but the projections which do not pass through or near metal implants are selectively used to reconstruct the artifact-free regions. This method is supposed to reduce edge effects and other errors that are missing in the model.

III.B.4. Hybrid sinogram correction

Combining different approaches to obtain a better performance by selecting suitable tools provided by each algorithm is quite common in various fields. In the context of MAR methods, several approaches have been proposed, in which a combination of interpolation-based sinogram correction, noninterpolation-based sinogram correction, and iterative image reconstruction techniques are used. In this section, we present hybrid MAR methods according to the following classification: (1) combination of interpolation-based and noninterpolation-based sinogram correction approaches, (2) combination of interpolation-based sinogram correction and iterative reconstruction, and (3) combination of noninterpolation-based sinogram correction and iterative reconstruction.

III.B.4.a. Combination of interpolation- and noninterpolation-based sinogram correction. A two-phase method was presented by Tuy.[120] In the first phase, metallic clips are localized using simple thresholding while the remaining pixels are set to −1000 HU. Forward projection of the obtained image generates the line integral of the clips only. The difference between the original sinogram and the clips-only sinogram (differential data) is then calculated, which represents the line integral of the whole object when the clips are removed. Linear interpolation is assumed to be a good estimate of the differential data within the projections passing through the clips. Therefore, in the case where the differential data are lower than linear interpolation of the unaffected data, the original data are modified by adding the difference between the linearly interpolated and differential data. This procedure compensates for the beam hardening effect in the original data and generates a high-contrast image. In the second phase, the image obtained in the first phase is used as a model to estimate the data along the projections passing through the clips. To ensure a proper transition of the data between the clip and nonclip regions, the affected projections are replaced by topological transposition of the values obtained by forward projection of the high-contrast image.

Another hybrid method, belonging to the first category, combines the linear interpolation technique and multidimensional adaptive filtering (MAF).[121] MAF is implemented according to the algorithm proposed by Kachelriess *et al*.[122] The noise-reduction property of MAF is more pronounced at larger distances from the metallic object. On the other hand, the linear interpolation introduces extra artifacts at larger distances. Therefore, these two approaches are combined by superimposing the resulting images where the pixels are weighted according to their distance from the metallic objects. In order to preserve the details in the reconstructed image, Jeong and Ra[123] merged the high-frequency components of the original sinogram and low-frequency components of the linearly interpolated sinogram.

A 3D correction approach was proposed by Prell *et al*.[124] where metallic objects are segmented followed by application of 3D linear interpolation to the corresponding projections. The reconstructed image is then classified into three materials including air, soft tissue and bone using a threshold-based method to produce a tissue-class model. Thereafter, the image model is forward projected to obtain the values of the corrupted projection bins. Abdoli *et al*. presented a MAR approach in which weighting coefficients, optimized by a genetic algorithm, are assigned to the original sinogram, spline interpolated sinogram and the neighboring column of the sinogram matrix.[85] The proposed approach makes use of the virtual sinogram concept.[125]

The idea of a hybrid nonlocal means inpainting and linear interpolation technique is developed by Li *et al.*[92] A similarity weighting function is defined to determine which replacement method should be used to replace the affected projections. If the weighting is larger than a fixed threshold, nonlocal means inpainting is used; otherwise, local linear interpolation is the method of choice.

The metal deletion technique (MDT) is an iterative approach in which the affected projections are replaced in an iterative forward projection procedure. In this method, the detector elements are expanded so that each element detects at least 30 photons. Thereafter, the initial image is constructed using linear interpolation. Then, FBP is iterated four times and in each iteration the affected projections are replaced by the values from the previous iteration.[119] Figure 6 presents a sample result of this group of hybrid MAR methods.[85] Compared to Fig. 4, it can be clearly seen that the visual quality of the corrected CT image is more satisfactory. Less smoothing and fewer extra artifacts are produced when using the hybrid MAR technique. Moreover, the attenuation corrected PET images show an effective reduction of overestimated tracer uptake after applying the hybrid MAR approach.

III.B.4.b. Combination of interpolation-based sinogram correction and iterative reconstruction. Nuyts and Stroobants combined linear interpolation and iterative reconstruction for MAR.[52] The image is first reconstructed using ML for transmission tomography[115] to reduce the artifacts to some extent. Thereafter, metallic objects are segmented using a thresholding technique and the metal traces, which are detected via forward projection of the segmented image, are replaced by linear interpolation. Metal traces are then multiplied by an arbitrary density and are added to the interpolated sinogram. The final image is generated by ML reconstruction. Metallic objects remain visible after correction because a density higher than the surrounding tissues is assigned to the corresponding projections. To reduce computing time for clinical application, the CT image size was downsampled to match the PET image.

A similar approach was proposed by Xia *et al.* who used B-spline interpolation followed by EM reconstruction technique.[126] Oehler and Buzug[127] presented an analogous method which makes use of a directional interpolation-based on the concept of image inpainting,[128] and reconstructed the image using a weighted ML-EM method. Cubic interpolation of the affected projections followed by penalized likelihood reconstruction of the corrected data was also proposed by Aootaphao *et al.*[129] A nonequispaced fast Fourier transform interpolation approach[130] followed by weighted ML-EM reconstruction is another related work proposed by Kratz and Buzug[131]

III.B.4.c. Combination of noninterpolation-based sinogram correction and iterative reconstruction. Lemmens *et al.* proposed a MAR method that uses maximum *a posteriori* (MAP) reconstruction[113] in combination with a projection completion approach.[132] First, an initial reconstruction of the CT image is performed using ML-TR. Thereafter, a constrained image is generated by incorporating *a priori* knowledge about attenuation coefficients of biological tissues. A thresholding approach is used to label the image components as belonging to patient's body, pixels which are likely to be affected by metal artifacts, and air or metal. An absolute intensity prior is defined for each label and the obtained prior together with Markov Gibbs prior is used for MAP reconstruction. The projection completion procedure is performed by replacing the affected projection bins in the original sinogram by those obtained from the MAP reconstruction. The corrected image is then reconstructed using the ML-TR algorithm.

Another hybrid method belonging to this category was recently presented.[133,134] In this approach, the projection data of an adjacent artifact-free CT slice is used to replace the affected projection bins of the corrupted slice. Since the adjacent images include roughly the same anatomical structure of the original image, they can be considered as a good approximation of the intact image. The corrected images are finally reconstructed using the ML-EM algorithm. Zhang

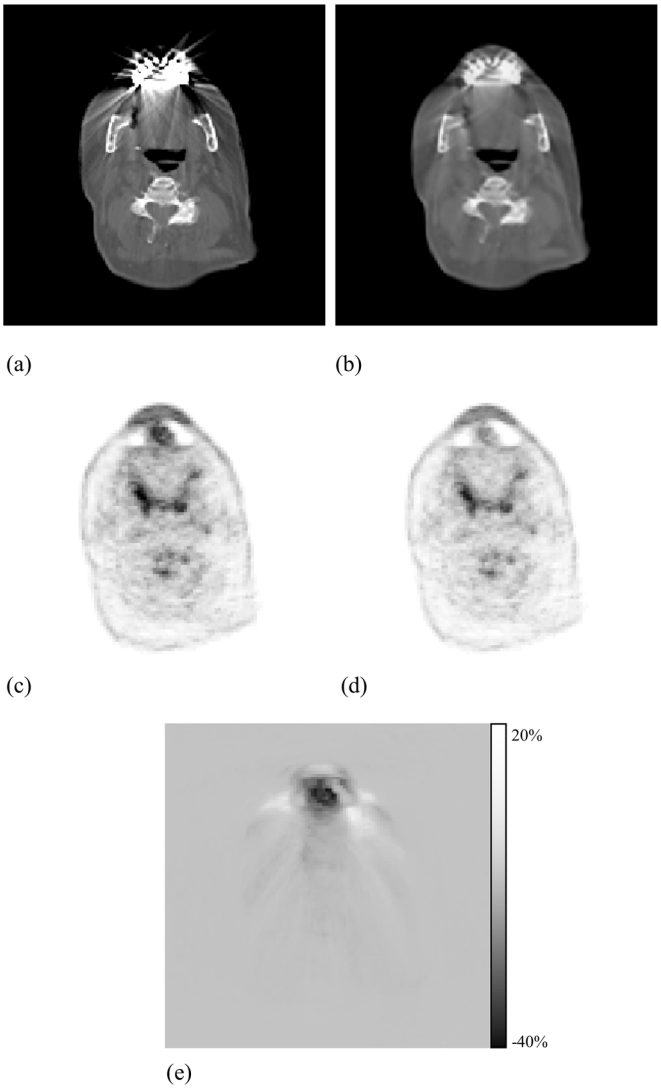

FIG. 6. A sample result of combination of interpolation-based and noninterpolation-based sinogram correction MAR methods (Ref. 85). (a) Original CT image including dental metallic artifact, (b) corrected CT image, (c) attenuation corrected PET data using image (a), (d) attenuation corrected PET data using image (b), and (e) subtraction of images (c) and (d).

et al. used a constrained optimization approach for MAR.[135] The image is first reconstructed using an iterative algorithm based on penalized weighted least-squares criterion. The metallic objects are then segmented and projected to define the affected projection bins. A constrained optimization model is then used for image reconstruction. In this optimization procedure, the estimated projection data have to be within a specified tolerance of the unaffected projection bins. A function reflecting *a priori* knowledge of the image is minimized by iteratively finding an image within the feasible region. A penalized smoothness objective is applied to evaluate the constrained optimization algorithm.

Figure 7 illustrates a representative example of this category of hybrid MAR approaches.[38] The reference image represents a slice not affected by metallic electrodes. The MAR approach has reduced the artifacts in CT and corresponding attenuation corrected PET images. The relative difference between the PET images corrected for attenuation using the reference CT and artifactual CT demonstrates that without applying the MAR algorithm, overestimation of tracer uptake appears in the whole image, but particularly in regions located at the position of the electrodes. After applying the MAR approach, however, the overestimations decrease. It must be emphasized that owing to the small size of the EEG electrodes in this example, and thus slight streaking artifacts, the influence of the artifacts on the PET image is not considerable.

III.B.5. Image-based approaches

As mentioned earlier, the majority of proposed MAR approaches manipulate the corrupted raw data to alleviate streaking artifacts visible on CT images. However, some

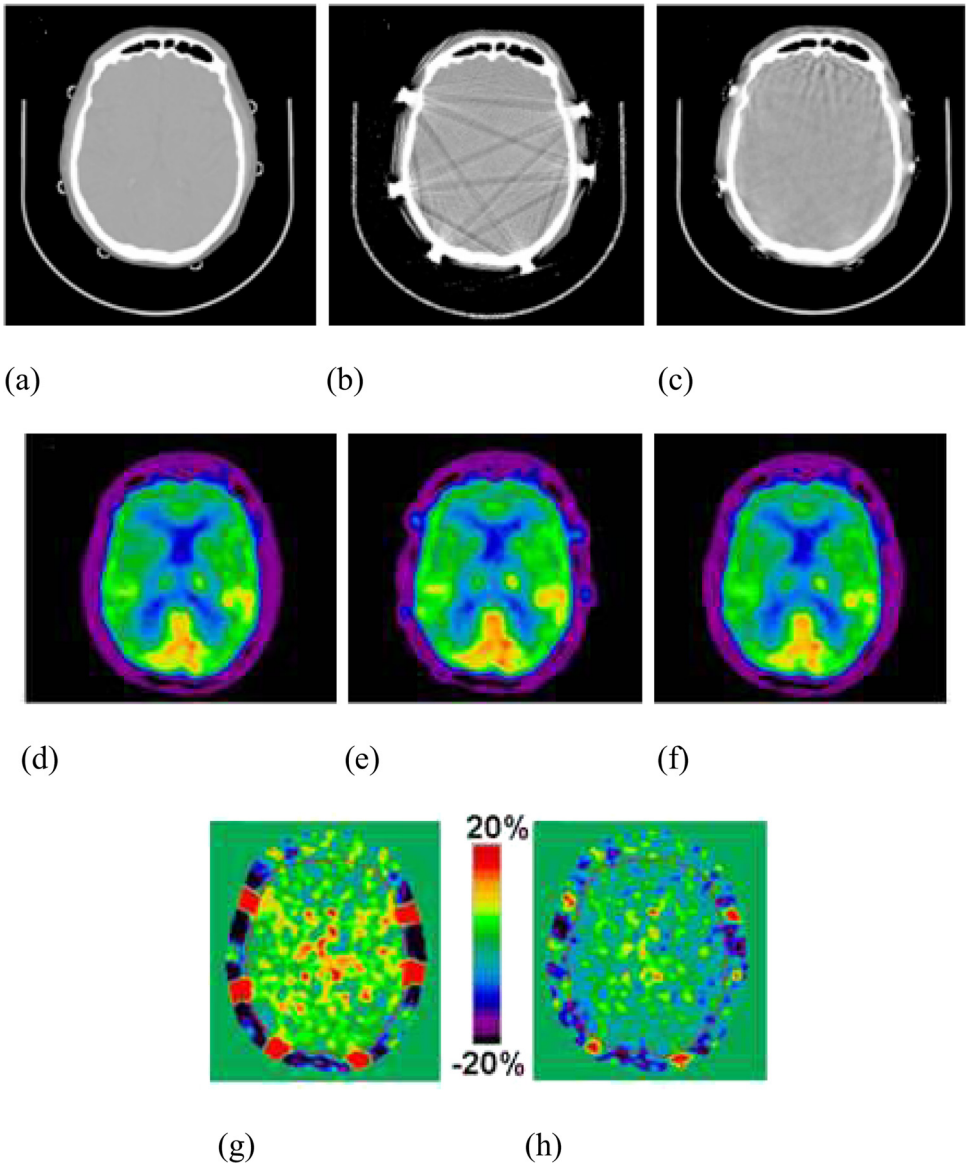

FIG. 7. A sample result of combination of noninterpolation-based sinogram correction MAR method and iterative reconstruction. (a) The CT reference image, (b) the uncorrected CT image including artifacts caused by metal electrodes, (c) the corrected CT image, (d) attenuation corrected PET data using image (a), (e) attenuation corrected PET data using image (b), (f) attenuation corrected PET data using image (c), (g) subtraction of images (d) and (e), and (h) subtraction of images (d) and (f). Reprinted with permission from C. Lemmens, M.-L. Montandon, J. Nuyts, O. Ratib, P. Dupont, and H. Zaidi, Phys. Med. Biol. **53**, 4417–4429 (2008). Copyright © 2008.

techniques deal with the problem in the image domain. Sohmura *et al*. used a dental cast model to replace regions of the jaw bone which are deteriorated by metallic artifacts.[136] This approach allows better visualization of the cranial bones for implant surgery. The CT images of the cast model and the patient's jaw are registered using an interface placed in the patient's mouth and in the cast model at the time of scanning. The position of the interface in both CT images facilitates the accurate registration of the images. The damaged regions of the bones in the original image are then replaced by the corresponding regions of the cast model. A qualitative comparison of PET images corrected for attenuation using original and segmented CT images was performed by Mirzaei *et al*.[137] Segmentation was carried out by dividing the CT image into three separate regions including lung, soft tissue and bone. To avoid the propagation of metallic artifacts to PET images, pixel values of regions with an intensity higher than the intensity of bone was assigned to the intensity of soft tissue. Their results suggest that segmented CT images result in better visual quality of attenuation corrected PET images. The quantitative impact of this approach, however, requires further investigation as pointed out by the authors.

A knowledge-based method was developed by Hamill *et al*.[138] The method was designed to reduce metallic artifacts produced by cardiac appliances based on known features of such artifacts. The MAR algorithm consists of six steps. First, CT images are rebinned to half of their original size to make the procedure faster. Thereafter, possible metal artifact regions are detected by thresholding to emphasize pixels having high intensity (M matrix). The threshold level segments the metallic object and the strong bright artifacts as well as bone structures. In order to include the dark artifact regions, the segmented image is dilated in three dimensions. The next step is to assign a range of values between zero and 100 to those pixels of the rebinned image which have a positive value. This procedure results in a smooth and continuous image in the positive range. Another binary matrix is formed by assigning a value of one to pixels with intensity equal to or greater than water density and zero to the rest (W matrix). This matrix undergoes a dilation followed by erosion to obtain smooth edges. Afterward, the dark streaking artifacts are defined as regions where the pixel value is lower than a specified threshold level, and the M and W matrices are set. Then, a positive value is assigned to the detected dark regions. Finally, after applying a median filter to eliminate the abrupt changes in isolated regions which are left in the last step, the CT image is expanded to its original size using bilinear interpolation.[85]

Another image-based MAR approach was presented by Kennedy *et al*.[37] The algorithm detects the metallic artifacts using a Bayes classifier applied around the pixels with maximum intensity in an annular region. A high threshold and a low threshold are determined in a phantom study to decide if the artifacts include bright streaks or dark ones. Thereafter, pixels belonging to dark regions are assigned CT number of soft tissue. Depending on the surrounding structures of the bright streaks, these regions will be assigned CT number of soft tissue or bone. This method was specifically designed to generate an attenuation map for CTAC of PET images. Recently, Naranjo *et al*. used morphological filtering in the polar domain for reduction of artifacts in the reconstructed image domain.[139] The original image is converted to a polar image by converting the Cartesian coordinates to polar coordinates. The polar image is then filtered using opening and closing morphological filters. The cavities in the original image are also segmented using simple thresholding and are preserved from the influence of filtering. The corrected image will be generated by combining the filtered image and the segmented image.

Figure 8 illustrates an example of this category of MAR methods.[138] It can be seen that, although the method is able to successfully correct for the overestimated regions of the PET image, it fails to correct the underestimation effects caused by dark streaking artifacts [arrows in Figs. 8(c) and 8(d)]. It should be mentioned that this MAR approach built-in Siemens PET/CT scanners (Siemens Healthcare, Erlangen, Germany) does not provide corrected CT images to the users. Therefore, only the original CT image and the uncorrected and corrected PET images are presented here.

IV. COMPARISON OF METAL ARTEFACT REDUCTION TECHNIQUES

As explained in Sec. III.A, implicit MAR techniques mainly manipulate the parameters that are responsible for generation of metallic artifacts prior to the scanning procedure. Such methods might be useful to reduce the disturbing effects of streaking artifacts or to prevent their generation to a limited extent in some special cases. However, due to their limited applicability, these methods cannot be considered as ultimate solutions for the metal artifact reduction. As a result, much worthwhile efforts aimed at developing mathematical concepts and algorithm capable of dealing appropriately with this adverse effect.

Among explicit approaches, sinogram-based methods have more attractive properties owing to the fact that the footprints of the streaks are more precisely traceable in the sinogram domain. In the sinogram domain, each projection bin contains the attenuation information of one line of response in the image domain. Therefore, detecting one pixel in the sinogram domain which is affected by metallic objects is equivalent to detecting one streaking line in the corresponding reconstructed image. However, the manipulation of the original raw CT data is usually cumbersome because of their large size and difficulties in reading proprietary encrypted format. This problem can be tackled using the virtual sinogram concept, which is obtained by forward projection of the reconstructed image.[125]

Interpolation techniques have been widely used as fast and straightforward approaches for MAR in the sinogram domain. Nevertheless, if the interpolation technique is not carefully selected, these methods can cause extra artifacts in the image. In particular, when one-dimensional interpolation schemes (mostly commonly used approach) are used, some inconsistencies might take place between the interpolated

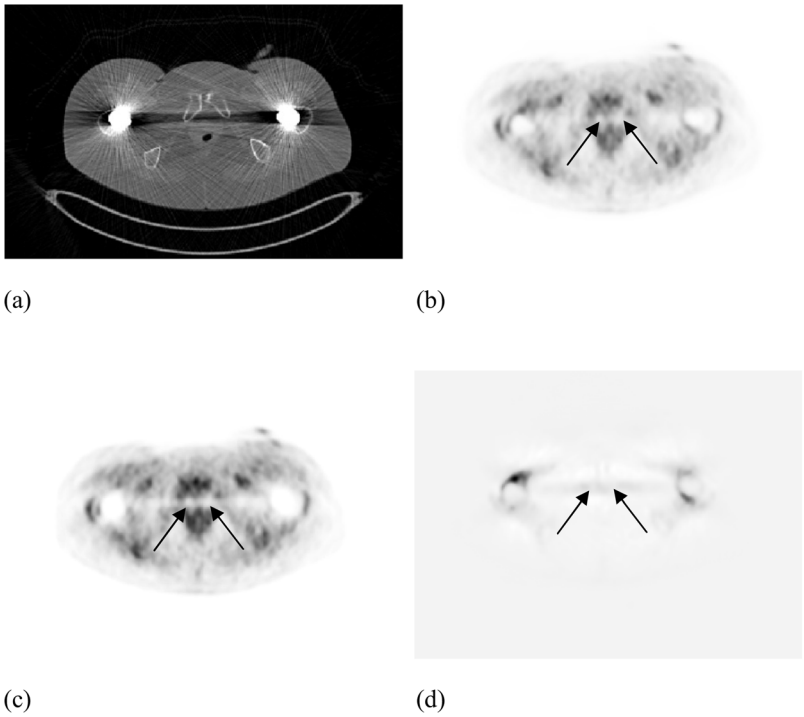

FIG. 8. Representative example of combination of image-based MAR methods (Ref. 138). (a) Original CT image including artifacts caused by hip implants, (b) attenuation corrected PET data using the image shown in (a), (c) attenuation corrected PET data using corrected CT image (not shown), and (d) subtraction of images shown in (b) and (c).

projection bins. These inconsistencies are responsible for the extra artifacts in the reconstructed image. These approaches are also likely to blur the anatomical structures around metallic objects. Moreover, the performance of an interpolation technique depends on the number of missing projection data. If the metallic object is bulky, a large number of projections would be influenced and less reliable data would be available to carry out the interpolation. Therefore, less accurate results would be obtained in such cases. However, owing to the simple and fast implementation of such techniques, the use of appropriate interpolation schemes combined with efficient optimization methods could result in a suitable MAR technique for use in clinical setting.

On the other hand, noninterpolation-based techniques include various approaches to replace the corrupted projection bins. These techniques use the surrounding pixels in the image domain to correct the sinogram by obtaining lower intensities of the affected bins to replace the original affected bins. The proposed methods provide acceptable artifact reduction of CT images. However, their influence on the attenuation corrected PET data has not been investigated. Figure 9 compares the results of a 1D linear interpolation approach and a noninterpolation-based approach.[99] It can be seen that the simple linear interpolation technique deteriorates image quality in regions adjacent to metallic objects. In contrast, noninterpolation-based approaches are more successful to preserve the structures in those regions.

An important issue regarding both interpolation- and noninterpolation-based approaches is worth mentioning. If the affected projection bins are simply replaced using an interpolation technique or by incorporating the surrounding unaffected bins and the CT image is used for attenuation correction of PET data, it is likely that this will lead to underestimation of tracer uptake in corresponding PET images. The reason is that metallic objects attenuate 511 keV photons more than other tissues, while when metallic objects are replaced by soft tissue in the CT image, this effect is being neglected and the attenuation is underestimated and, thus, the tracer uptake will be underestimated as well. This problem was tackled by inserting the actual CT number of the metallic object in the reconstructed CT image in order to correctly estimate photon attenuation at 511 keV.[75–77,80] An alternative to account for this effect consists of adding a term to the corrected projection bins to generate CT numbers close to that of the metallic object in the reconstructed image.[74,87]

Iterative reconstruction is an appropriate alternative to FBP, which due to mishandling of noise, results in visible streaking artifacts. MAR approaches which make use of iterative reconstruction apply different approaches to handle the problem of incomplete and noisy projection data. Some methods assign a lower weight to the affected projection bins to reduce their troublous impact.[113] Other approaches modify the affected projection bins and then iterative reconstruction is carried out.[116] There are also a number of other approaches in which the low-count projections are directly used by the reconstruction procedure.[108–110] The main concern regarding such techniques is the high computational time. However, resampling the raw CT data to PET resolution might reduce the computational time to a clinically acceptable range.[52] One must be aware of the information loss during the resampling procedure which might result in less accurate data correction. Moreover, the performance of iterative algorithms is highly influenced by CT system configurations and the quality of projection data, which can be considered as another limitation of such techniques.[135] It should also be emphasized that iterative reconstruction is not the ultimate solution for metal streaking artifacts since

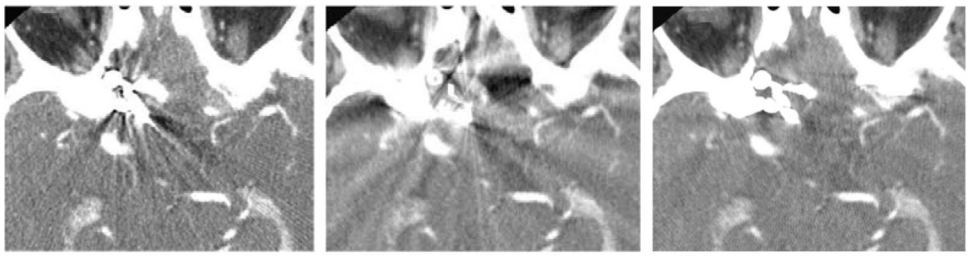

FIG. 9. Comparison between a linear interpolation MAR approach and a noninterpolation-based method. (a) Original CT image, (b) CT image corrected by linear interpolation, and (c) CT image corrected by a noninterpolation-based approach. Reprinted with permission from M. Bal and L. Spies, Med. Phys. **33**, 2852–2859 (2006). Copyright © 2006.

photon starvation is not the only cause of these artifacts as discussed in Sec. II.

Hybrid techniques are usually of interest because of their capability to compensate for a single method's shortcomings. Hybrid methods which combine interpolation and noninterpolation-based approaches seem to be more beneficial since combining them with iterative methods does not solve the high computation time and costs associated with iterative approaches. As can be seen in Fig. 6, this type of hybrid MAR methods is more successful to retain the anatomical structures around the metallic objects. Moreover, the qualitative and quantitative influence of artifact reduction on attenuation corrected PET images is more pronounced. Figure 10 compares a combination of interpolation- and noninterpolation-based methods[123] with a 1D linear interpolation technique. Although both methods are not able to successfully restore the image, the hybrid method preserves more details in the image.

Combination of interpolation-based and noninterpolation-based approaches with iterative reconstruction techniques has shown to improve the quality of the corrected CT image compared to methods using FBP reconstruction. On the other hand, the inherent limitations of iterative approaches still hold. The quantitative impact of such methods when used for CTAC of PET images has not been fully characterized. Figure 11 compares the combination of interpolation-based and iterative reconstruction approaches[131] with a 1D linear interpolation method in the sinogram domain. Note the discontinuities between the projection bins generated by 1D interpolation schemes. The hybrid method, however, results in a smooth sinogram. Figure 12 illustrates the difference between linear and polynomial interpolation techniques and a combination of noninterpolation-based and iterative reconstruction approaches.[132] The superiority of the hybrid method over interpolation-based methods is clearly observable. This is in contrast with the results of the phantom study performed by Rinkel *et al.*[140] in which no significant difference between interpolation-based methods[34,35,75] and the combination of interpolation-based and noninterpolation-based approaches was reported.[121] In another study by Boas and Fleischmann, an iterative method (SART), a hybrid method (MDT), and linear interpolation were compared.[119] It has been reported that MDT, which combines noninterpolation and interpolation-based approaches, is superior to iterative and interpolation-based techniques. This puts forward the importance of benchmarking and confirms the necessity of evaluation of MAR methods using clinical datasets.

The main obstacle associated with image-based MAR techniques is the fuzziness of CT numbers in regions influenced by artifacts and the surrounding regions. This fuzziness makes the differentiation between metallic objects, artifactual regions and the surrounding tissues complicated and might give rise to inferior performance. Furthermore, methods belonging to this category usually replace the values of the affected pixels by a constant value, which might degrade image quality to a great extent. Nevertheless, this limitation might not cause a serious problem when CT images are only used for attenuation correction purposes. On the other hand, some image-based MAR methods only account for the bright streaking artifacts. Therefore, such methods

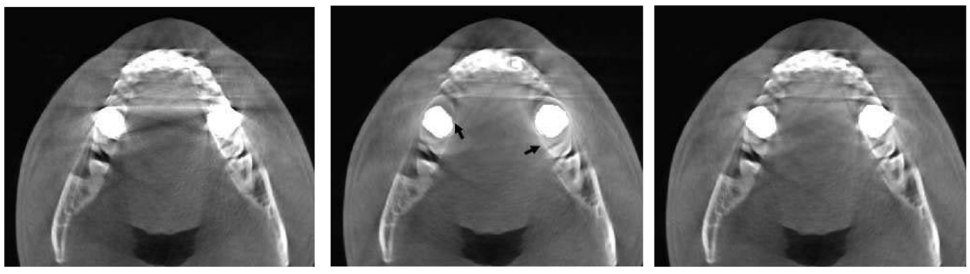

FIG. 10. Comparison between a linear interpolation MAR approach and a combination of interpolation- and noninterpolation-based methods. (a) Original CT image, (b) CT image corrected by linear interpolation, (c) CT image corrected by the hybrid approach. Reprinted with permission from K. Y. Jeong and J. B. Ra, "Metal artifact reduction based on sinogram correction in CT," in IEEE Nuclear Science Symposium and Medical Imaging Conference (Orlando, FL, 2009), pp. 3480–3483. © 2009 IEEE.

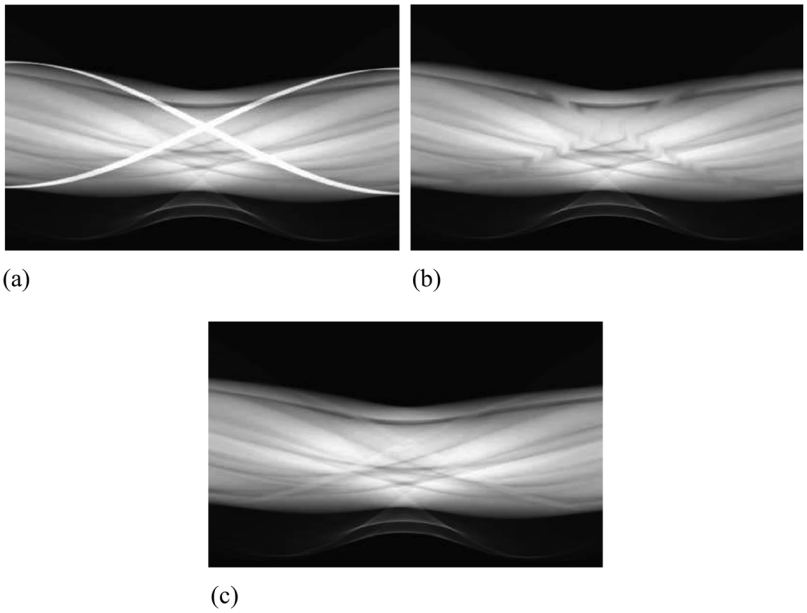

FIG. 11. Comparison between a linear interpolation MAR approach and a combination of interpolation-based and iterative reconstruction methods in sinogram space. (a) Original sinogram, (b) sinogram corrected by linear interpolation, (c) sinogram corrected by the hybrid approach. Reprinted with permission from B. Kratz and T. M. Buzug, "Metal artifact reduction in computed tomography using nonequispaced Fourier transform," in IEEE Nuclear Science Symposium Conference Record (Orlando, FL, 2009), pp. 2720–2723. © 2009 IEEE.

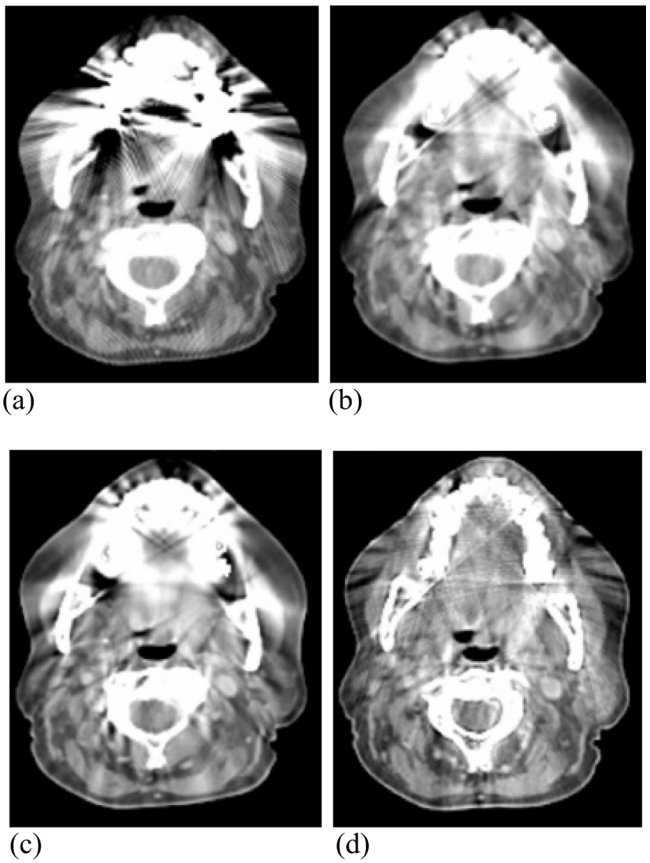

FIG. 12. Comparison between a linear interpolation MAR approach and a combination of noninterpolation- based and iterative reconstruction methods. (a) Original CT image, (b) CT image corrected by linear interpolation, (c) CT image corrected by polynomial interpolation, (d) CT image corrected by the hybrid approach. Reprinted with permission from C. Lemmens, D. Faul and J. Nuyts, "Suppression of metal artifacts in CT using a reconstruction procedure that combines MAP and projection completion," IEEE Trans Med Imaging **28**, 250–260 (2009) © 2009 IEEE.

leave the dark artifacts unchanged, and as such, potential underestimations in the corresponding attenuation corrected PET data remain unchanged (Fig. 8).

Evaluation of MAR algorithms has always been a challenging issue in clinical setting owing to the lack of ground truth. The usual assessment strategy consists of visual examination which has inherent limitations related to the subjectivity of the observer. Recently, a reference-free ground truth metric for CT images was introduced by Kratz *et al.*[141] This approach considers the subset of the original raw data, which are not affected by metallic objects, as the inherent ground truth. This information is then used to evaluate the degree of artifacts by comparing the original projection data with those obtained by forward projection of the reconstructed CT images.

V. CONCLUSION

Several studies have reported the adverse impact of metallic artifacts on CT images and their influence on CT-based attenuation corrected PET images. With the exception of metallic implants of small size, which might generate slight streaking artifacts, metallic objects usually cause severe bright and dark streaks in CT images and overestimation and/or underestimation of tracer uptake in corresponding attenuation corrected PET images. Reduction of such artifacts can help to improve clinical diagnosis, to assess response to therapy, surgery and radiation therapy planning, prognosis assessment, and above all enable accurate quantification.

The various categories of MAR methods have shown variable performance in artifact reduction of CT images. However, only a few of methods have been applied to hybrid PET/CT imaging, and among those, some approaches have been only quantitatively assessed for clinical usage. Nevertheless, virtually all MAR methods developed exclusively for improving diagnostic CT images can be adapted for application in hybrid PET/CT imaging. It should be

emphasized that, in case of hybrid PET/CT imaging, the diagnostic quality of CT images is not the main issue. The issue is to generate an accurate attenuation map to enable accurate attenuation correction of PET data. On the other hand, algorithmic complexity and computational time are significant factors influencing clinical applicability of MAR algorithms. In this respect, MAR methods incorporating iterative reconstruction techniques might not be clinically relevant owing to the fact that very high quality CT images are not required for attenuation correction purposes. Moreover, the high computational time associated with iterative procedures might hinder clinical applicability of these techniques. However, if this limitation can be appropriately dealt with, iterative reconstruction should be preferred to FBP.

In general, sinogram-based MAR approaches have been shown to be more accurate to obtain reliable attenuation coefficients. Interpolation-based techniques can be considered as a fast remedy for replacement of affected projection bins. Combination of interpolation and noninterpolation-based approaches is a more suitable option for improvement of the performance of such methods. The quantitative assessment of MAR approaches applied to PET/CT images is still required for comparison between the available techniques and selection of the most appropriate option.

ACKNOWLEDGMENTS

This work was supported by the Swiss National Science Foundation under grant SNSF 31003A-135576, Geneva Cancer League, the Indo-Swiss Joint Research Programme ISJRP 138866, Geneva University Hospital under grant PRD 11-II-1, and a research grant from Siemens Healthcare.

[a]Author to whom correspondence should be addressed. Electronic mail: habib.zaidi@hcuge.ch; Telephone: +41 22 372 7258; Fax: +41 22 372 7169.

[1]W. A. Kalender, "X-ray computed tomography," Phys. Med. Biol. **51**, R29–R43 (2006).
[2]T. M. Blodgett, C. C. Meltzer, and D. W. Townsend, "PET/CT: Form and function," Radiology **242**, 360–385 (2007).
[3]H. Zaidi, H. Vees, and M. Wissmeyer, "Molecular PET/CT imaging-guided radiation therapy treatment planning," Acad. Radiol. **16**, 1108–1133 (2009).
[4]H. Zaidi and I. El Naqa, "PET-guided delineation of radiation therapy treatment volumes: A survey of image segmentation techniques," Eur. J. Nucl. Med. Mol. Imaging **37**, 2165–2187 (2010).
[5]M. E. Juweid and B. D. Cheson, "Positron-emission tomography and assessment of cancer therapy," N. Engl. J. Med. **354**, 496–507 (2006).
[6]G. K. von Schulthess and N. J. Pelc, "Integrated-modality imaging: The best of both worlds," Acad. Radiol. **9**, 1241–1244 (2002).
[7]J. A. Patton, D. W. Townsend, and B. F. Hutton, "Hybrid imaging technology: From dreams and vision to clinical devices," Semin. Nucl. Med. **39**, 247–263 (2009).
[8]G. W. Goerres, G. K. von Schulthess, and H. C. Steinert, "Why most PET of lung and head-and-neck cancer will be PET/CT," J. Nucl. Med. **45**, 66S–71S (2004).
[9]H. Schoder, S. M. Larson, and H. W. D. Yeung, "PET/CT in oncology: Integration into clinical management of lymphoma, melanoma, and gastrointestinal malignancies," J. Nucl. Med. **45**, 72S–81S (2004).
[10]R. L. Wahl, "Why nearly all PET of abdominal and pelvic cancers will be performed as PET/CT," J. Nucl. Med. **45**, 82S–95S (2004).
[11]J. Czernin, M. Allen-Auerbach, and H. R. Schelbert, "Improvements in cancer staging with PET/CT: Literature-based evidence as of September 2006," J. Nucl. Med. **48**, 78S–88 (2007).
[12]A. Constantinidou, A. Martin, B. Sharma, and S. R. Johnston, "Positron emission tomography/computed tomography in the management of recurrent/metastatic breast cancer: A large retrospective study from the Royal Marsden Hospital," Ann. Oncol. **22**, 307–314 (2011).
[13]B. Hasegawa and H. Zaidi, "Dual-modality imaging: More than the sum of its components," in *Quantitative Analysis in Nuclear Medicine Imaging*, edited by H. Zaidi (Springer, New York, 2006), pp. 35–81.
[14]D. W. Townsend, "Multimodality imaging of structure and function," Phys. Med. Biol. **53**, R1–R39 (2008).
[15]P. E. Kinahan, D. W. Townsend, T. Beyer, and D. Sashin, "Attenuation correction for a combined 3D PET/CT scanner," Med. Phys. **25**, 2046–2053 (1998).
[16]C. Bai, P. E. Kinahan, D. Brasse, C. Comtat, D. W. Townsend, C. C. Meltzer, V. Villemagne, M. Charron, and M. Defrise, "An analytic study of the effects of attenuation on tumor detection in whole-body PET oncology imaging," J. Nucl. Med. **44**, 1855–1861 (2003).
[17]H. Zaidi and B. H. Hasegawa, "Determination of the attenuation map in emission tomography," J. Nucl. Med. **44**, 291–315 (2003).
[18]O. Mawlawi, T. Pan, and H. A. Macapinlac, "PET/CT imaging techniques, considerations, and artifacts," J. Thorac. Imaging **21**, 99–110 (2006).
[19]C. Burger, G. Goerres, S. Schoenes, A. Buck, A. H. Lonn, and G. K. Von Schulthess, "PET attenuation coefficients from CT images: Experimental evaluation of the transformation of CT into PET 511-keV attenuation coefficients," Eur. J. Nucl. Med. Mol. Imaging **29**, 922–927 (2002).
[20]H. Zaidi, M.-L. Montandon, and A. Alavi, "Advances in attenuation correction techniques in PET," PET Clin. **2**, 191–217 (2007).
[21]J. A. van Dalen, W. V. Vogel, F. H. Corstens, and W. J. Oyen, "Multimodality nuclear medicine imaging: Artefacts, pitfalls and recommendations," Cancer Imaging **7**, 77–83 (2007).
[22]W. Sureshbabu and O. Mawlawi, "PET/CT imaging artifacts," J. Nucl. Med. Technol. **33**, 156–161 (2005).
[23]T. M. Blodgett, A. S. Mehta, C. M. Laymon, J. Carney, and D. W. Townsend, "PET/CT artifacts," Clin. Imaging **35**, 49–63 (2011).
[24]S. A. Nehmeh and Y. E. Erdi, "Respiratory motion in positron emission tomography/computed tomography: A review," Semin. Nucl. Med. **38**, 167–176 (2008).
[25]J. A. Nye, F. Esteves, and J. R. Votaw, "Minimizing artifacts resulting from respiratory and cardiac motion by optimization of the transmission scan in cardiac PET/CT," Med. Phys. **34**, 1901–1906 (2007).
[26]A. Rahmim, O. Rousset, and H. Zaidi, "Strategies for motion tracking and correction in PET," PET Clin. **2**, 251–266 (2007).
[27]E. Klotz, W. A. Kalender, R. Sokiransky, and D. Felsenberg, "Algorithms for the reduction of CT artifacts caused by metallic implants," Proc. SPIE **1234**, 642–650 (1990).
[28]H. Zaidi, M.-L. Montandon, and S. Meikle, "Strategies for attenuation compensation in neurological PET studies," Neuroimage **34**, 518–541 (2007).
[29]S. J. Rosenbaum, T. Lind, G. Antoch, and A. Bockisch, "False-positive FDG PET uptake—The role of PET/CT," Eur. Radiol. **16**, 1054–1065 (2006).
[30]G. J. Cook, E. A. Wegner, and I. Fogelman, "Pitfalls and artifacts in 18FDG PET and PET/CT oncologic imaging," Semin. Nucl. Med. **34**, 122–133 (2004).
[31]A. Bockisch, T. Beyer, G. Antoch, L. S. Freudenberg, H. Kuhl, J. F. Debatin, and S. P. Muller, "Positron emission tomography/computed tomography—Imaging protocols, artifacts, and pitfalls," Mol. Imaging Biol. **6**, 188–199 (2004).
[32]A. M. Alessio, P. E. Kinahan, P. M. Cheng, H. Vesselle, and J. S. Karp, "PET/CT scanner instrumentation, challenges, and solutions," Radiol. Clin. North Am. **42**, 1017–1032, vii (2004).
[33]A. Croxford, P. Fajnwaks, C. Botkin, D. Oliver, N. Nguyen, and M. Osman, "Prevalence and patterns of metal artifacts in FDG PET/CT," J. Nucl. Med. **51**, 2123 (2010).
[34]D. D. Robertson, J. Yuan, G. Wang, and M. W. Vannier, "Total hip prosthesis metal-artifact suppression using iterative deblurring reconstruction," J. Comput. Assist. Tomogr. **21**, 293–298 (1997).
[35]W. A. Kalender, R. Hebel, and J. Ebersberger, "Reduction of CT artifacts caused by metallic implants," Radiology **164**, 576–577 (1987).
[36]E. M. Kamel, C. Burger, A. Buck, G. K. von Schulthess, and G. W. Goerres, "Impact of metallic dental implants on CT-based attenuation correction in a combined PET/CT scanner," Eur. Radiol. **13**, 724–728 (2003).

[37]J. A. Kennedy, O. Israel, A. Frenkel, R. Bar-Shalom, and H. Azhari, "The reduction of artifacts due to metal hip implants in CT-attenuation corrected PET images from hybrid PET/CT scanners," Med. Biol. Eng. Comput. **45**, 553–562 (2007).
[38]C. Lemmens, M.-L. Montandon, J. Nuyts, O. Ratib, P. Dupont, and H. Zaidi, "Impact of metal artefacts due to EEG electrodes in brain PET/CT imaging," Phys. Med. Biol. **53**, 4417–4429 (2008).
[39]S. L. Bowen, Y. Wu, A. J. Chaudhari, L. Fu, N. J. Packard, G. W. Burkett, K. Yang, K. K. Lindfors, D. K. Shelton, R. Hagge, A. D. Borowsky, S. R. Martinez, J. Qi, J. M. Boone, S. R. Cherry, and R. D. Badawi, "Initial characterization of a dedicated breast PET/CT scanner during human imaging," J. Nucl. Med. **50**, 1401–1408 (2009).
[40]A. J. Duerinckx and A. Macovski, "Polychromatic streak artifacts in computed tomography images," J. Comput. Assist. Tomogr. **2**, 481–487 (1978).
[41]G. H. Glover, "Compton scatter effects in CT reconstructions," Med. Phys. **9**, 860–867 (1982).
[42]A. J. Duerinckx and A. Macovski, "Nonlinear polychromatic and noise artifacts in x-ray computed tomography images," J. Comput. Assist. Tomogr. **3**, 519–526 (1979).
[43]G. H. Glover and N. J. Pelc, "Nonlinear partial volume artifacts in x-ray computed tomography," Med. Phys. **7**, 238–248 (1980).
[44]G. H. Glover and N. J. Pelc, "An algorithm for the reduction of metal clip artifacts in CT reconstructions," Med. Phys. **8**, 799–807 (1981).
[45]B. De Man, J. Nuyts, P. Dupont, G. Marchal, and P. Suetens, "Metal streak artifacts in x-ray computed tomography: A simulation study," IEEE Trans. Nucl. Sci. **46**, 691–696 (1999).
[46]R. A. Brooks and G. Di Chiro, "Beam hardening in x-ray reconstructive tomography," Phys. Med. Biol. **21**, 390–398 (1976).
[47]J. Hsieh, "Nonlinear partial volume artifact correction in helical CT," IEEE Trans. Nucl. Sci. **46**, 743–747 (1999).
[48]B. De Man, Ph.D. Thesis, Katholieke Universiteit Leuven, 2001.
[49]G. W. Goerres, S. I. Ziegler, C. Burger, T. Berthold, G. K. Von Schulthess, and A. Buck, "Artifacts at PET and PET/CT caused by metallic hip prosthetic material," Radiology **226**, 577–584 (2003).
[50]N. Subhas, P. V. Patel, H. K. Pannu, H. A. Jacene, E. K. Fishman, and R. L. Wahl, "Imaging of pelvic malignancies with in-line FDG PET-CT: Case examples and common pitfalls of FDG PET," Radiographics **25**, 1031–1043 (2005).
[51]M. R. Ay, A. Mehranian, M. Abdoli, P. Ghafarian, and H. Zaidi, "Qualitative and quantitative assessment of metal artifacts arising from implantable cardiac pacing devices in oncological PET/CT studies: A phantom study," Mol. Imaging Biol. **13**, 1077–1087 (2011).
[52]J. Nuyts and S. Stroobants, "Reduction of attenuation correction artifacts in PET-CT," in *IEEE Nuclear Science Symposium Conference Record* (Puerto Rico, 2005), Vol. 4, pp. 1895–1899.
[53]C. Nahmias, C. Lemmens, D. Faul, E. Carlson, M. Long, T. Blodgett, J. Nuyts, and D. Townsend, "Does reducing CT artifacts from dental implants influence the PET interpretation in PET/CT studies of oral cancer and head and neck cancer?," J. Nucl. Med. **49**, 1047–1052 (2008).
[54]G. W. Goerres, T. F. Hany, E. Kamel, G. K. von Schulthess, and A. Buck, "Head and neck imaging with PET and PET/CT: Artefacts from dental metallic implants," Eur. J. Nucl. Med. Mol. Imaging **29**, 367–370 (2002).
[55]K. P. Schafers, R. Raupach, and T. Beyer, "Combined 18F-FDG-PET/CT imaging of the head and neck. An approach to metal artifact correction," Nuklearmedizin **45**, 219–222 (2006).
[56]H. Shimamoto, N. Kakimoto, K. Fujino, S. Hamada, E. Shimosegawa, S. Murakami, S. Furukawa, and J. Hatazawa, "Metallic artifacts caused by dental metal prostheses on PET images: A PET/CT phantom study using different PET/CT scanners," Ann. Nucl. Med. **23**, 443–449 (2009).
[57]H. J. Griffiths, D. R. Priest, D. M. Kushner, and D. Kushner, "Total hip replacement and other orthopedic hip procedures," Radiol. Clin. North Am. **33**, 267–287 (1995).
[58]C. Cyteval, V. Hamm, M. P. Sarrabere, F. M. Lopez, P. Maury, and P. Taourel, "Painful infection at the site of hip prosthesis: CT imaging," Radiology **224**, 477–483 (2002).
[59]P. T. Liu, W. P. Pavlicek, M. B. Peter, M. J. Spangehl, C. C. Roberts, and R. G. Paden, "Metal artifact reduction image reconstruction algorithm for CT of implanted metal orthopedic devices: A work in progress," Skeletal Radiol. **38**, 797–802 (2009).
[60]K. D. Stumpe, H. P. Notzli, M. Zanetti, E. M. Kamel, T. F. Hany, G. W. Gorres, G. K. von Schulthess, and J. Hodler, "FDG PET for differentiation of infection and aseptic loosening in total hip replacements: Comparison with conventional radiography and three-phase bone scintigraphy," Radiology **231**, 333–341 (2004).
[61]S. I. Heiba, J. Luo, S. Sadek, E. Macalental, A. Cacavio, G. Rosen, and H. A. Abdel-Dayem, "Attenuation-correction induced artifact in F-18 FDG PET imaging following total knee replacement," Clin. Positron Imaging **3**, 237–239 (2000).
[62]F. P. DiFilippo and R. C. Brunken, "Do implanted pacemaker leads and ICD leads cause metal-related artifact in cardiac PET/CT?," J. Nucl. Med. **46**, 436–443 (2005).
[63]P. Ghafarian, S. M. Aghamiri, M. R. Ay, A. Rahmim, T. H. Schindler, O. Ratib, and H. Zaidi, "Is metal artefact reduction mandatory in cardiac PET/CT imaging in the presence of pacemaker and implantable cardioverter defibrillator leads?," Eur. J. Nucl. Med. Mol. Imaging **38**, 252–262 (2011).
[64]Y. Kim, W. A. Tome, M. Bal, T. R. McNutt, and L. Spies, "The impact of dental metal artifacts on head and neck IMRT dose distributions," Radiother. Oncol. **79**, 198–202 (2006).
[65]Y. Kim and W. A. Tome, "On the radiobiological impact of metal artifacts in head-and-neck IMRT in terms of tumor control probability (TCP) and normal tissue complication probability (NTCP)," Med. Biol. Eng. Comput. **45**, 1045–1051 (2007).
[66]J. F. Barrett and N. Keat, "Artifacts in CT: Recognition and avoidance," Radiographics **24**, 1679–1691 (2004).
[67]C. Coolens and P. J. Childs, "Calibration of CT Hounsfield units for radiotherapy treatment planning of patients with metallic hip prostheses: The use of the extended CT-scale," Phys. Med. Biol. **48**, 1591–1603 (2003).
[68]I. S. Lee, H. J. Kim, B. K. Choi, Y. J. Jeong, T. H. Lee, T. Y. Moon, and D. Won Kang, "A pragmatic protocol for reduction in the metal artifact and radiation dose in multislice computed tomography of the spine: Cadaveric evaluation after cervical pedicle screw placement," J. Comput. Assist. Tomogr. **31**, 635–641 (2007).
[69]S. G. Moon, S. H. Hong, J. Y. Choi, W. S. Jun, H. G. Kang, H. S. Kim, and H. S. Kang, "Metal artifact reduction by the alteration of technical factors in multidetector computed tomography: A 3-dimensional quantitative assessment," J. Comput. Assist. Tomogr. **32**, 630–633 (2008).
[70]F. Bamberg, A. Dierks, K. Nikolaou, M. F. Reiser, C. R. Becker, and T. R. Johnson, "Metal artifact reduction by dual energy computed tomography using monoenergetic extrapolation," Eur. Radiol. **21**, 1424–1429 (2011).
[71]W. S. Park, K. D. Kim, H. K. Shin, and S. H. Lee, "Reduction of metal artifact in three-dimensional computed tomography (3D CT) with dental impression materials," in *Conference Proceedings of IEEE Engineering in Medicine and Biology Society* (Lyon, France, 2007), pp. 3496–3499.
[72]R. M. Lewitt and R. H. T. Bates, "Image reconstruction from projections: III Projection completion methods (theory)," Optik **50**, 189–204 (1978).
[73]T. Hinderling, P. Ruegsegger, M. Anliker, and C. Dietschi, "Computed tomography reconstruction from hollow projections: An application to *in vivo* evaluation of artificial hip joints," J. Comput. Assist. Tomogr. **3**, 52–57 (1979).
[74]S. Zhao, D. D. Robertson, G. Wang, B. Whiting, and K. T. Bae, "X-ray CT metal artifact reduction using wavelets: An application for imaging total hip prostheses," IEEE Trans. Med. Imaging **19**, 1238–1247 (2000).
[75]A. H. Mahnken, R. Raupach, J. E. Wildberger, B. Jung, N. Heussen, T. G. Flohr, R. W. Gunther, and S. Schaller, "A new algorithm for metal artifact reduction in computed tomography: *In vitro* and *in vivo* evaluation after total hip replacement," Invest. Radiol. **38**, 769–775 (2003).
[76]J. C. Roeske, C. Lund, C. A. Pelizzari, X. Pan, and A. J. Mundt, "Reduction of computed tomography metal artifacts due to the Fletcher-Suit applicator in gynecology patients receiving intracavitary brachytherapy," Brachytherapy **2**, 207–214 (2003).
[77]J. Wei, L. Chen, G. A. Sandison, Y. Liang, and L. X. Xu, "X-ray CT high-density artefact suppression in the presence of bones," Phys. Med. Biol. **49**, 5407–5418 (2004).
[78]M. Yazdi, L. Gingras, and L. Beaulieu, "An adaptive approach to metal artifact reduction in helical computed tomography for radiation therapy treatment planning: Experimental and clinical studies," Int. J. Radiat. Oncol., Biol., Phys. **62**, 1224–1231 (2005).
[79]J. Gu, L. Zhang, G. Yu, Y. Xing, and Z. Chen, "X-ray CT metal artifacts reduction through curvature based sinogram inpainting," J. X-Ray Sci. Technol. **14**, 73–82 (2006).

[80]M. Bazalova, L. Beaulieu, S. Palefsky, and F. Verhaegen, "Correction of CT artifacts and its influence on Monte Carlo dose calculations," Med. Phys. **34**, 2119–2132 (2007).
[81]H. Yu, K. Zeng, D. K. Bharkhada, G. Wang, M. T. Madsen, O. Saba, B. Policeni, M. A. Howard, and W. R. Smoker, "A segmentation-based method for metal artifact reduction," Acad. Radiol. **14**, 495–504 (2007).
[82]Y. Zhang, L. Zhang, X. R. Zhu, A. K. Lee, M. Chambers, and L. Dong, "Reducing metal artifacts in cone-beam CT images by preprocessing projection data," Int. J. Radiat. Oncol., Biol., Phys. **67**, 924–932 (2007).
[83]X. Duan, L. Zhang, Y. Xiao, J. Cheng, Z. Chen, and Y. Xing, "Metal artifact reduction in CT images by sinogram TV inpainting," in *IEEE Nuclear Science Symposium Conference Record*, (Dresden, Germany, 2008), pp. 4175–4177.
[84]L. Yu, H. Li, J. Mueller, J. M. Kofler, X. Liu, A. N. Primak, J. G. Fletcher, L. S. Guimaraes, T. Macedo, and C. H. McCollough, "Metal artifact reduction from reformatted projections for hip prostheses in multislice helical computed tomography: Techniques and initial clinical results," Invest. Radiol. **44**, 691–696 (2009).
[85]M. Abdoli, M. Ay, A. Ahmadian, R. Dierckx, and H. Zaidi, "Reduction of dental filling metallic artefacts in CT-based attenuation correction of PET data using weighted virtual sinograms optimized by a genetic algorithm," Med. Phys. **37**, 6166–6177 (2010).
[86]Y. Kim, S. Yoon, and J. Yi, "Effective sinogram-inpainting for metal artifacts reduction in X-ray CT images," in *17th IEEE International Conference on Image Processing (ICIP)* (Hong Kong, 2010), pp. 597–600.
[87]W. J. H. Veldkamp, R. M. S. Joemai, A. J. van der Molen, and J. Geleijns, "Development and validation of segmentation and interpolation techniques in sinograms for metal artifact suppression in CT," Med. Phys. **37**, 620–628 (2010).
[88]C. Xu, F. Verhaegen, D. Laurendeau, S. A. Enger, and L. Beaulieu, "An algorithm for efficient metal artifact reductions in permanent seed," Med. Phys. **38**, 47–56 (2011).
[89]R. M. Lewitt and R. H. T. Bates, "Image reconstruction from projections: IV: Projection completion methods (computational examples)," Optik **50**, 269–278 (1978).
[90]M. Abdoli, J. R. de Jong, J. Pruim, R. A. Dierckx, and H. Zaidi, "Reduction of artefacts caused by hip implants in CT-based attenuation-corrected PET images using 2-D interpolation of a virtual sinogram on an irregular grid," Eur. J. Nucl. Med. Mol. Imaging **38**, 2257–2268 (2011).
[91]M. Yazdi and L. Beaulieu, "A novel approach for reducing metal artifacts due to metallic dental implants," in *IEEE Nuclear Science Symposium Conference Record* (San Diego, CA, 2006), pp. 2260–2263.
[92]H. Li, L. Yu, X. Liu, J. G. Fletcher, and C. H. McCollough, "Metal artifact suppression from reformatted projections in multislice helical CT using dual-front active contours," Med. Phys. **37**, 5155–5164 (2010).
[93]E. Meyer, R. Raupach, M. Lell, B. Schmidt, and M. Kachelriess, "Normalized metal artifact reduction (NMAR) in computed tomography," Med. Phys. **37**, 5482–5493 (2010).
[94]C. Steger, "An unbiased detector of curvilinear structures," IEEE Trans. Pattern Anal. Mach. Intell. **20**, 113–125 (1998).
[95]A. Mehranian, M. R. Ay, A. Rahmim, and H. Zaidi, "Sparsity constrained sinogram inpainting for metal artifact reduction in x-ray computed tomography," in *IEEE Nuclear Science Symposium and Medical Imaging Conference* (Valencia, Spain, 2011), pp. 3694–3699.
[96]R. Morin and D. Raeside, "A pattern recognition method for the removal of streaking artifact in computed tomography," Radiology **141**, 229–233 (1981).
[97]J. K. Dixon, "Pattern recognition with partly missing data," IEEE Trans. Syst. Man. Cybern. **9**, 617–621 (1979).
[98]J. J. Liu, S. R. Watt-Smith, and S. M. Smith, "CT reconstruction using FBP with sinusoidal amendment for metal artifact reduction," in *VIIth Digital Image Computing* (Sydney, Australia, 2003), pp. 10–12.
[99]M. Bal and L. Spies, "Metal artifact reduction in CT using tissue-class modeling and adaptive prefiltering," Med. Phys. **33**, 2852–2859 (2006).
[100]J. Wu, C.-T. Shih, S.-J. Chang, T.-C. Huang, J.-Y. Sun, and T.-H. Wu, "Metal artifact reduction algorithm based on model images and spatial information," Nucl. Instrum. Methods A **652**, 602–605 (2011).
[101]L. Cheng and J. Liu, "Metal artifacts reduction in computed tomography: A bilateral reprojection approach," in *4th International Conference on Bioinformatics and Biomedical Engineering (iCBBE)* (Chengdu, China, 2010), pp. 1–4.
[102]A. Mehranian, M. R. Ay, A. Rahmim, and H. Zaidi, "Metal artifact reduction in CT-based attenuation correction of PET using Sobolev sinogram restoration," in *IEEE Nuclear Science Symposium and Medical Imaging Conference* (Valencia, Spain, 2011), pp. 2936–2942.
[103]X. Pan, E. Y. Sidky, and M. Vannier, "Why do commercial CT scanners still employ traditional, filtered back-projection for image reconstruction?," Inverse Probl. **25**, 123009 (2009).
[104]E. T. Quinto, "Tomographic reconstructions from incomplete data-numerical inversion of the exterior Radon transform," Inverse Probl. **4**, 867–876 (1988).
[105]M. Defrise and G. T. Gullberg, "Image reconstruction," Phys. Med. Biol. **51**, R139–154 (2006).
[106]A. C. Kak and M. Slaney, "Algebraic reconstruction algorithms," in *Principles of Computerized Tomographic Imaging* (IEEE, New York, 1999), pp. 275–296.
[107]L. A. Shepp and Y. Vardi, "Maximum likelihood reconstruction for emission tomography," IEEE Trans. Med. Imaging **1**, 113–122 (1982).
[108]K. Lange and R. Carson, "EM reconstruction algorithms for emission and transmission tomography," J. Comput. Assist. Tomogr. **8**, 306–316 (1984).
[109]G. Wang, D. L. Snyder, J. A. O'sullivan, and M. W. Vannier, "Iterative deblurring for CT metal artifact reduction," IEEE Trans. Med. Imaging **15**, 657–664 (1996).
[110]G. Wang, M. W. Vannier, and P. C. Cheng, "Iterative x-ray cone-beam tomography for metal artifact reduction and local region reconstruction," Microsc. Microanal. **5**, 58–65 (1999).
[111]G. Wang, T. Frei, and M. W. Vannier, "Fast iterative algorithm for metal artifact reduction in x-ray CT," Acad. Radiol. **7**, 607–614 (2000).
[112]D. L. Snyder, J. A. O'sullivan, B. R. Whiting, R. J. Murphy, J. Benac, J. A. Cataldo, D. G. Politte, and J. F. Williamson, "Deblurring subject to nonnegativity constraints when known functions are present with application to object-constrained computerized tomography," IEEE Trans. Med. Imaging **20**, 1009–1017 (2001).
[113]B. De Man, J. Nuyts, P. Dupont, G. Marchal, and P. Suetens, "Reduction of metal streak artifacts in x-ray computed tomography using a transmission maximum *a posteriori* algorithm," IEEE Trans. Nucl. Sci. **47**, 977–981 (2000).
[114]E. U. Mumcuoglu, R. M. Leahy, and S. R. Cherry, "Bayesian reconstruction of PET images: Methodology and performance analysis," Phys. Med. Biol. **41**, 1777–1807 (1996).
[115]J. Nuyts, B. De Man, P. Dupont, M. Defrise, P. Suetens, and L. Mortelmans, "Iterative reconstruction for helical CT: A simulation study," Phys. Med. Biol. **43**, 729–737 (1998).
[116]J. Hsieh, R. C. Molthen, C. A. Dawson, and R. H. Johnson, "An iterative approach to the beam hardening correction in cone beam CT," Med. Phys. **27**, 23–29 (2000).
[117]J. F. Williamson, B. R. Whiting, J. Benac, R. J. Murphy, G. J. Blaine, J. A. O'sullivan, D. G. Politte, and D. L. Snyder, "Prospects for quantitative computed tomography imaging in the presence of foreign metal bodies using statistical image reconstruction," Med. Phys. **29**, 2404–2418 (2002).
[118]J. A. O'sullivan and J. Benac, "Alternating minimization algorithms for transmission tomography," IEEE Trans. Med. Imaging **26**, 283–297 (2007).
[119]F. E. Boas and D. Fleischmann, "Evaluation of two iterative techniques for reducing metal artifacts in computed tomography," Radiology **259**, 894–902 (2011).
[120]H. K. Tuy, "A post-processing algorithm to reduce metallic clip artifacts in CT images," Eur. Radiol. **V3**, 129–134 (1993).
[121]O. Watzke and W. A. Kalender, "A pragmatic approach to metal artifact reduction in CT: Merging of metal artifact reduced images," Eur. Radiol. **14**, 849–856 (2004).
[122]M. Kachelriess, O. Watzke, and W. A. Kalender, "Generalized multi-dimensional adaptive filtering for conventional and spiral single-slice, multi-slice, and cone-beam CT," Med. Phys. **28**, 475–490 (2001).
[123]K. Y. Jeong and J. B. Ra, "Metal artifact reduction based on sinogram correction in CT," in *IEEE Nuclear Science Symposium Conference Record* (Orlando, FL, 2009), pp. 3480–3483.
[124]D. Prell, Y. Kyriakou, M. Beister, and W. A. Kalender, "A novel forward projection-based metal artifact reduction method for flat-detector computed tomography," Phys. Med. Biol. **54**, 6575–6591 (2009).
[125]M. Abdoli, M. R. Ay, A. Ahmadian, and H. Zaidi, "A virtual sinogram method to reduce dental metallic implant artefacts in computed tomography-based attenuation correction for PET," Nucl. Med. Commun. **31**, 22–31 (2010).

[126]D. Xia, J. C. Roeske, L. Yu, C. A. Pelizzari, A. J. Mundt, and X. Pan, "A hybrid approach to reducing computed tomography metal artifacts in intracavitary brachytherapy," Brachytherapy **4**, 18–23 (2005).
[127]M. Oehler and T. M. Buzug, "The λ-MLEM Algorithm: An iterative reconstruction technique for metal artifact reduction in CT images," in *Advances in Medical Engineering* (Springer, Berlin, 2007), Vol. 114, pp. 42–47.
[128]M. Bertalmio, G. Sapiro, V. Caselles and C. Ballester, "Image inpainting," in *Proceedings of the 27th Aannual Conference on Computer Graphics and Interactive Techniques* (ACM/Addison-Wesley, 2000).
[129]S. Aootaphao, C. Pintavirooj, and S. Sotthivirat, "Penalized-likelihood reconstruction for metal artifact reduction in cone-beam CT," in *Conference Proceedings of IEEE Engineering in Medicine and Biology Society* (Vancouver, British Columbia, Canada, 2008), pp. 2733–2736.
[130]B. Kratz, T. Knopp, J. Müller, M. Oehler, T. M. Buzug, T. Tolxdorff, J. Braun, T. M. Deserno, A. Horsch, H. Handels, and H.-P. Meinzer, "Non-equispaced Fourier transform vs. polynomial-based metal artifact reduction in Computed Tomography," in Bildverarbeitung für die Medizin (Springer Berlin, Heidelberg, 2008), pp. 21–25.
[131]B. Kratz and T. M. Buzug, "Metal artifact reduction in computed tomography using nonequispaced Fourier transform," in *IEEE Nuclear Science Symposium Conference Record* (Orlando, FL, 2009), pp. 2720–2723.
[132]C. Lemmens, D. Faul, and J. Nuyts, "Suppression of metal artifacts in CT using a reconstruction procedure that combines MAP and projection completion," IEEE Trans. Med. Imaging **28**, 250–260 (2009).
[133]A. Kondo, Y. Hayakawa, J. Dong, and A. Honda, "Iterative correction applied to streak artifact reduction in an x-ray computed tomography image of the dento-alveolar region," Oral Radiol. **26**, 61–65 (2010).
[134]J. Dong, A. Kondo, K. Abe, and Y. Hayakawa, "Successive iterative restoration applied to streak artifact reduction in x-ray CT image of dento-alveolar region," Int. J. Comput. Assist. Radiol. Surg. **6**, 635–640 (2011).
[135]X. Zhang, J. Wang, and L. Xing, "Metal artifact reduction in x-ray computed tomography (CT) by constrained optimization," Med. Phys. **38**, 701–711 (2011).
[136]T. Sohmura, H. Hojoh, N. Kusumoto, M. Nishida, K. Wakabayashi, and J. Takahashi, "A novel method of removing artifacts because of metallic dental restorations in 3-D CT images of jaw bone," Clin. Oral Implants Res. **16**, 728–735 (2005).
[137]S. Mirzaei, M. Guerchaft, C. Bonnier, P. Knoll, M. Doat, and P. Braeutigam, "Use of segmented CT transmission map to avoid metal artifacts in PET images by a PET-CT device," BMC Nucl. Med. **5**, 3 (2005).
[138]J. J. Hamill, R. C. Brunken, B. Bybel, F. P. DiFilippo, and D. D. Faul, "A knowledge-based method for reducing attenuation artefacts caused by cardiac appliances in myocardial PET/CT," Phys. Med. Biol. **51**, 2901–2918 (2006).
[139]V. Naranjo, R. Llorens, M. Alcaniz, and F. Lopez-Mir, "Metal artifact reduction in dental CT images using polar mathematical morphology," Comput. Methods Programs Biomed. **102**, 64–74 (2011).
[140]J. Rinkel, W. P. Dillon, T. Funk, R. Gould, and S. Prevrhal, "Computed tomographic metal artifact reduction for the detection and quantitation of small features near large metallic implants: A comparison of published methods," J. Comput. Assist. Tomogr. **32**, 621–629 (2008).
[141]B. Kratz, S. Ens, J. Muller, and T. M. Buzug, "Reference-free ground truth metric for metal artifact evaluation in CT images," Med. Phys. **38**, 4321–4328 (2011).